AD-A156 577 THE GENERATION AND TRANSMISSION OF VIBRATION IN PLAIN CYLINDRICAL BEARING..(U) ADMIRALTY MARINE TECHNOLOGY ESTABLISHMENT TEDDINGTON (ENGLAND.. L V EMBLING ET AL. 1/1

UNCLASSIFIED SEP 84 AMTE(N)/R84009 DRIC-BR-95891 F/G 13/9 NL

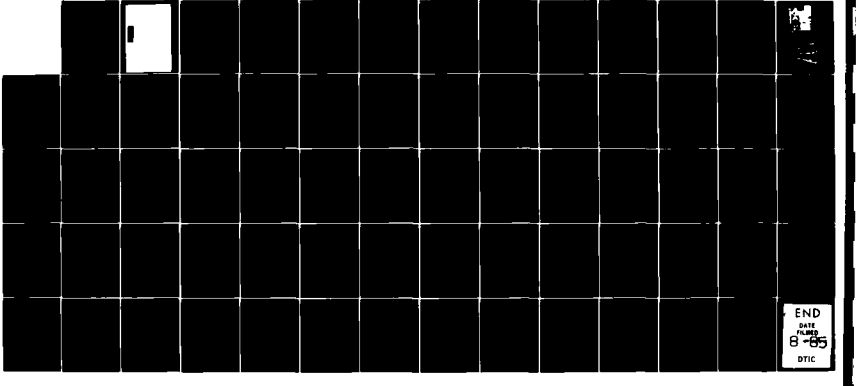

END
DATE FILMED
8-85
DTIC

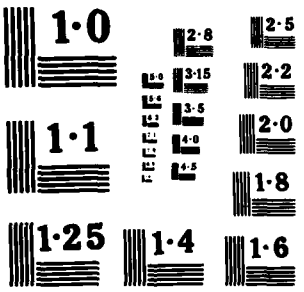
1·0
1·1
1·25
1·4
1·6
1·8
2·0
2·2
2·5
2·8
3·15
3·5
4·0
4·5
5·0

AMTE(N) R 84009

THE GENERATION AND TRANSMISSION OF VIBRATION IN PLAIN CYLINDRICAL BEARINGS (U)

PART 2. EXPERIMENT

L.V. EMBLING, C.J. JENKINS and P. MEYER.

SUMMARY

The vibration transmission characteristics of hydrodynamic bearings have been investigated at frequencies well above the out of balance frequency. Part 1 of this report developed theories to predict the linear transfer functions of bearings and to examine the effects of non linearities in modulating the response to external forces. This part of the report describes an experimental investigation on a bearing test rig aimed at validating the theories.

It is concluded that i) bearings are not always rigid to vibration, the frequency range over which rigidity applies being determined by the bearing parameters; ii) Transfer functions across the bearing in the direction of the applied force are reciprocal; and iii) The bearing can introduce modulation in the response to a single-frequency force.

Structural properties; vibration; oil flow; Great Britain

Addition of keywords: Europe, engines,

68 pages
24 figures

ARE(TEDDINGTON)
Queen's Road
TEDDINGTON
Middlesex TW11 OLN

September 1984

CONTENTS

1. INTRODUCTION

In the past little work seems to have been directed at bearing transmission properties and conflicting conclusions have been reached. Whereas White [1] concluded that the bearings are rigid, Kinns [2] assumed that the oil film inertance is low compared with that of the bearing so that the housing response to excitation due to out of balance is very much less than that of the rotor. One aim of this work was to resolve such differences of opinion.

A second aim of the work was to investigate the modulation of vibration induced by non-linear effects on transmission across the bearing. It has been suggested that such effects could account for the shaft rate modulations which have been observed on various gear tones on marine gearboxes [3].

Part 1 of the report of this work [3, also described in 4] reviewed previous work which had been directed mainly at bearing behaviour around shaft rate and developed the theory to describe the vibration properties of "long" and "short" 360; and 180; hydrodynamic bearings at frequencies well above shaft rate. The case of the "long" 360; bearing was considered in more detail to assess i) the effects of perturbations on the bearing surfaces in generating vibrations within the bearing, ii) the linear transfer functions and iii) the effects of non-linearity in modulating the transmitted vibrations. It was concluded that
i)if the surface roughness is described as a series of harmonic terms in azimuth angle then for low eccentricity bearings only the low harmonic components will generate significant forces within the bearing,
ii) the bearing is rigid in the direction of the applied force at frequencies above shaft rate unless a) the bearing stiffness is low compared with that of the housing, (if the housing behaviour is governed by its stiffness) or b), the bearing stiffness is low compared with the housing mass multiplied with the shaft and forcing frequencies (when the housing behaviour is governed by its mass);
iii) the sidebands due to modulation will be some 80dB or more down on the fundamental when the bearing is very stiff.

This report reviews previous experimental work on bearing vibration characteristics (section 3) and describes a test rig which has been built to measure the transfer functions and to investigate the occurrence of modulation (section 4).

The structural properties of the rig when static and the bearing parameters when running at different shaft rates are explored (sections 6 and 7). These results are used to predict the linear transfer functions of the test bearing using the theory developed previously [3,4] (section 8). Measured linear transfer functions are presented and compared with these predictions (section 9) and the occurrence of modulation is investigated (section 10).

2. NOTATION

R	Test bearing radius
L	Test bearing length
c	Test bearing clearance
m_j	Journal mass
m_h	Housing mass
k	Housing stiffness
K	Bearing stiffness $K=A\Omega/2c$
F_0	Static load $(m_j g)$
ω	Angular frequency of dynamic force
Ω	Angular frequency of journal
U	Tangential velocity of journal. $U=R\Omega$
n	Eccentricity ratio
ρ	Density of oil
η	Kinematic viscosity of oil
μ	Absolute viscosity of oil $\mu=\rho\eta$
A	$12\mu R^3 L\pi/c^2$
Q	Oil flow rate
P_0	Oil feed pressure
h	Oil film thickness $h=c(1+n\cos\theta)$
x_j, y_j	Displacements of journal
y_j, y_h	Displacements of housing

3. REVIEW OF PREVIOUS EXPERIMENTAL INVESTIGATIONS.

A comprehensive review of work on the dynamics of fluid bearings up until 1965 is given in [5] and need not be repeated here. It is sufficient to say that this early work established the major sources of vibration in hydrodynamic bearings to be rotor unbalance and fluid film whirl. (These effects are briefly described in Appendix 1.) Since 1965 researchers have continued to concentrate on these effects while very little work seems to have been done on the transmission of vibration across the bearing.

Although the results of previous work are not always of direct relevance to the present study the experimental test rigs used provide useful ideas, some of which have been incorporated in the design of the test rig for this investigation. It therefore seems appropriate at this stage to consider briefly some of the preceding experiments.

HOLMES [7] investigated the frequency and amplitude characteristics of steady oil whirl both theoretically (using the stiffness and damping coefficients of the oil film for the "long" and "short" 360° bearing) and experimentally. He used a perspex bearing and journal for simple manufacture and reduced extraneous stiffness by employing a special drive coupling and by eliminating oil seals. The bearing had a length to diameter ratio of around unity and a large clearance ratio was used to reduce the temperature of the lubricant. To ensure a full film at high eccentricity low bearing pressures were used. The oil was gravity fed into a central circumferential groove and allowed to run out at the bearing ends; this meant there was a large axial component to the oil flow so that the short bearing approximation applied.

BANNISTER [8] investigated the orbital response of 120° partial bearings to out of balance forces of varying frequency and considered the effects of misalignment. He concluded that non-linearities in the bearing coefficients had to be accounted for to effect agreement between theory and experiment.

The main features of the experimental test rig are shown in Figure 1a. The dynamic loading was provided by a system of out of balance forces inside the test journal; this consisted of two sets of out of balance masses attached to rotating discs on an inner shaft supported on ball bearings and driven independently of the test journal to provide out of balance forces at varying frequencies. The static loading and misalignment were applied by pneumatic pistons at both ends of the bearing. Displacement probes were used to sense the orbit of the test journal.

WHITE [1] measured the transfer characteristics of various types of bearing including 360° hydrodynamic bearings and concluded that under normal operating conditions such bearings would have no effect on the transmitted signals.

The test rig used a three bearing configuration as shown in Figure 1b, the reaction load for the central test bearing being taken symmetrically by the outer support bearings. To allow the latter to support the journal at low or zero speed and to minimise extraneous vibrations pressurised hydrostatic bearings were chosen.

A static load was applied to the test bearing housing by means of a loading frame with strain gauges attached and the dynamic load was applied to the housing through a force transducer by using an electrodynamic shaker. Proximity probes installed in the bearing housing allowed the shaft orbit to be monitored but dynamic displacements of the shaft were too small to be

measured in this way. The transfer response was therefore measured at the support bearing housing; the test bearing transfer characteristics were deduced by correcting the measured response to allow for the response of the rest of the rig which was measured with the test bearing depleted of oil.

PARKINS [9] used a similar test rig to that of White [7] to investigate the non-linearities of the oil film coefficients. In this case torsion wires were used to provide vertical and horizontal static loads on the test bearing with the corresponding dynamic loads being applied through electromagnetic shakers. Oil was supplied to the centre of the test bearing and allowed to drain through the ends. Transverse locating wires were used during dynamic tests to prevent axial motion of the bearing housing relative to the shaft.

FLACK and ROOKE [10] investigated the synchronous unbalance response of a flexible rotor in different types of fluid film bearings. The test rig consisted of a flexible shaft with three closely mounted discs located mid-way between two bearing supports. The main interest of this work was in the effects of shaft flexibility since this is an important factor affecting the operation of industrial machinery which had previously received little attention in bearing studies.

COOKSON and KOSSA [11] assessed the effectiveness of squeeze film damper bearings in reducing the rotor vibration amplitude and the force transmitted to the bearing housing. In its simplest form the squeeze film damper bearing consists of a fluid filled annulus around the outer race of a rolling contact bearing; this race is prevented from rotating but can orbit around the centre of rotation "squeezing" a pressure film ahead of it. (The squeeze film effect is discussed in section 2 of Part 1 [3].) This work has a close but not direct relationship to the present study of hydrodynamic bearings.

The test rig consisted of a flexible shaft with a steel disc situated midway between two rolling contact bearings with interchangeable squeeze film dampers. Rings with equispaced holes were attached to either side of the disc in order to facilitate balancing.

This is by no means a complete discussion of the relevant experimental work but it does indicate that the vibration transmission characteristics have not received much attention and provides useful experience for building a test rig for this purpose.

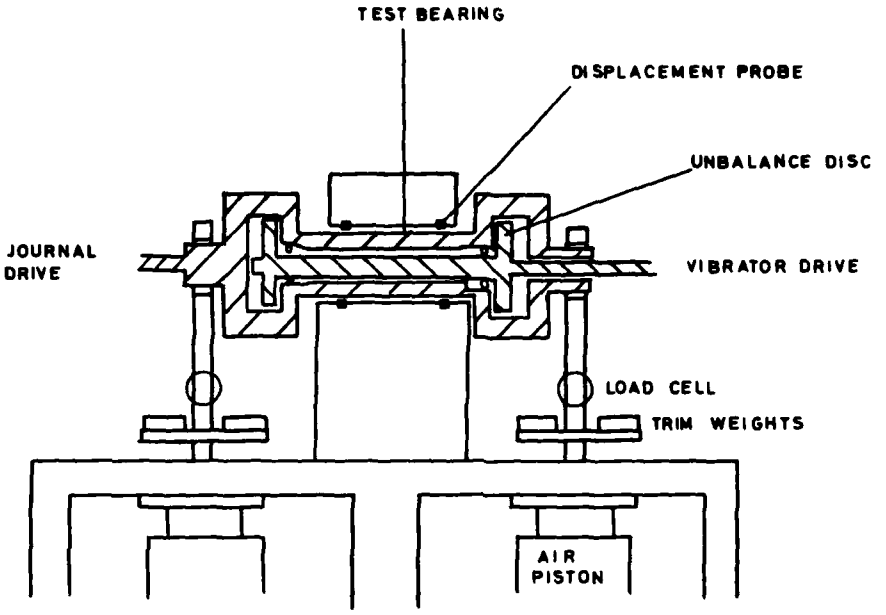

FIG. 1a BANNISTER'S [6] UNBALANCE AND MISALIGNMENT TEST RIG

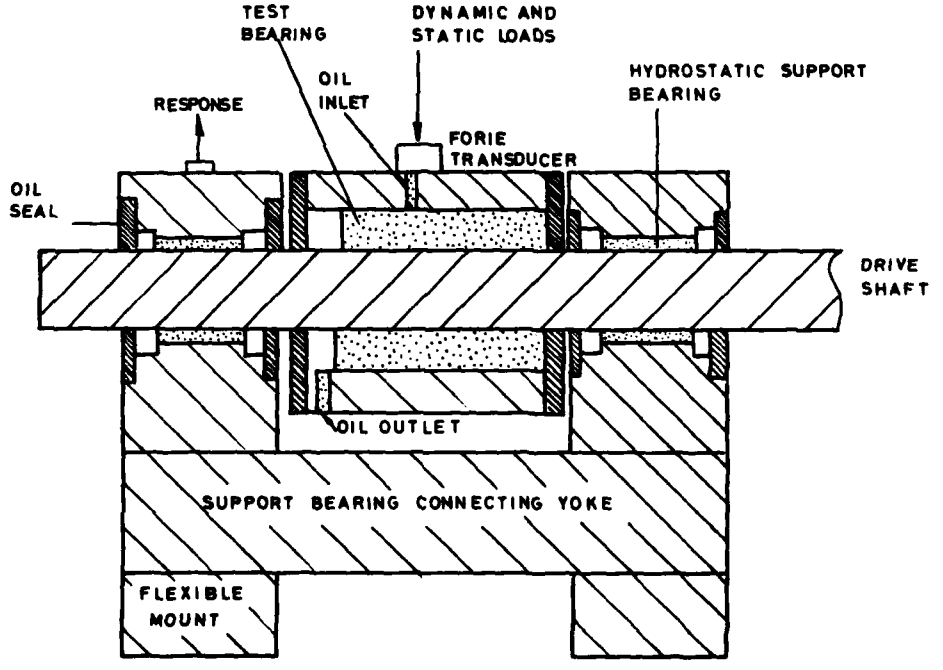

FIG. 1b WHITE'S [7] BEARING VIBRATION TRANSMISSION RIG

4. DESIGN OF BEARING TEST RIG

Since the aim of the work was to isolate the transfer characteristics of the bearing, the test rig was designed so far as possible to minimise the effects of extraneous transmission mechanisms. It was decided that a three bearing configuration like that used by White [1] should be avoided due to possible complications introduced by the transmission of the vibration through the rotor and across the support bearing. An arrangement similar in concept to that used by Bannister [8] was therefore adopted.

The test rig is shown in Figure 2 and Plates 1 and 2. It consists essentially of a plain bearing machined out of a solid steel block which is supported on an "A" frame construction mounted on the test bed. The bearing supports a journal which is belt driven from a variable speed motor using a system of two symetrically placed belts at each end of the rotor. The shaft rate was measured using an optical tachometer.

In order to allow a known dynamic force to be applied to the journal within the length of the bearing, the journal was hollow and, since the force could not conveniently be applied to a rotating surface, a stationary hollow shaft supported by an inner bearing was inserted. Although the transfer functions would now be measured across two bearings, the inner bearing was made very stiff compared with the test bearing so that transmission effects across the former could be neglected. As a precaution, displacement probes were inserted to measure the relative displacement across the inner bearing to verify that any movement was comparatively small.

Lip seals were used at the ends of both bearings; these were intended to suppress axial flow of the oil so that the "long" bearing approximation could be applied. The oil was gravity fed via inlet holes into the bearings from a common supply about a metre above the rig and was allowed to drain from the inner bearing via holes in the rotor and then from the test bearing through pairs of circumferential grooves. Two types of oil were used with widely differing viscosities in order to allow variation of the oil film stiffness. These were a Naval diesel lubricating oil, SAE 30, - with joint service designation OMD113, and a general purpose lubricating oil - designation OM 13. The temperature of the oil was monitored by thermocouples placed at the inlet to the test bearing and at the combined outlet.

A variable static load was applied symmetrically to the ends of the stator via W mounts.A dynamic force was applied through a force transducer to the inside of the stator via a pivoted lever driven by a shaker standing on the test bed. In order to investigate reciprocity a second dynamic force was applied at the top of the housing but this had to be off-centred due to the driving mechanism. The accelerations were measured on the inner stator and housing block as indicated in Figure 2 and, so long as the inner bearing and the housing behaved rigidly, these were taken to represent the responses at the bearing surfaces.

The basic design parameters for the test rig are listed in Table 1.

TABLE 1. DESIGN PARAMETERS OF BEARING TEST RIG.

Test Bearing	Radius	R		5.0cm
	Length	L		10.0cm
	* Clearance	c		0.5mm
Inner bearing	Radius			3.5cm
	Length			10.0cm
	* Clearance			0.1mm
Stator inner radius				2.9cm
Housing mass		m_h		44kg
Stator mass				5kg
Effective journal mass		m_j		20kg
Loading mass below mounts	m_l	"low load"		12kg
		"high load"	OMD113	62kg
			OMD13	32kg
Total static load	$F_o=(m_j+m_l)g$	"low load"		320N
		"high load"	OMD113	820N
			OMD13	620N
Diameter of oil inlet hole		D		5.0mm
± Housing stiffness		k_y		3.2×10^7 Nm^{-1}
		k_x		1.2×10^7 Nm^{-1}

* Clearance decreases on running rig due to thermal expansion of metallic components. See Table 3 for estimated values under running conditions.

± As measured from point inertance.

∝ Nominal, can be varied.

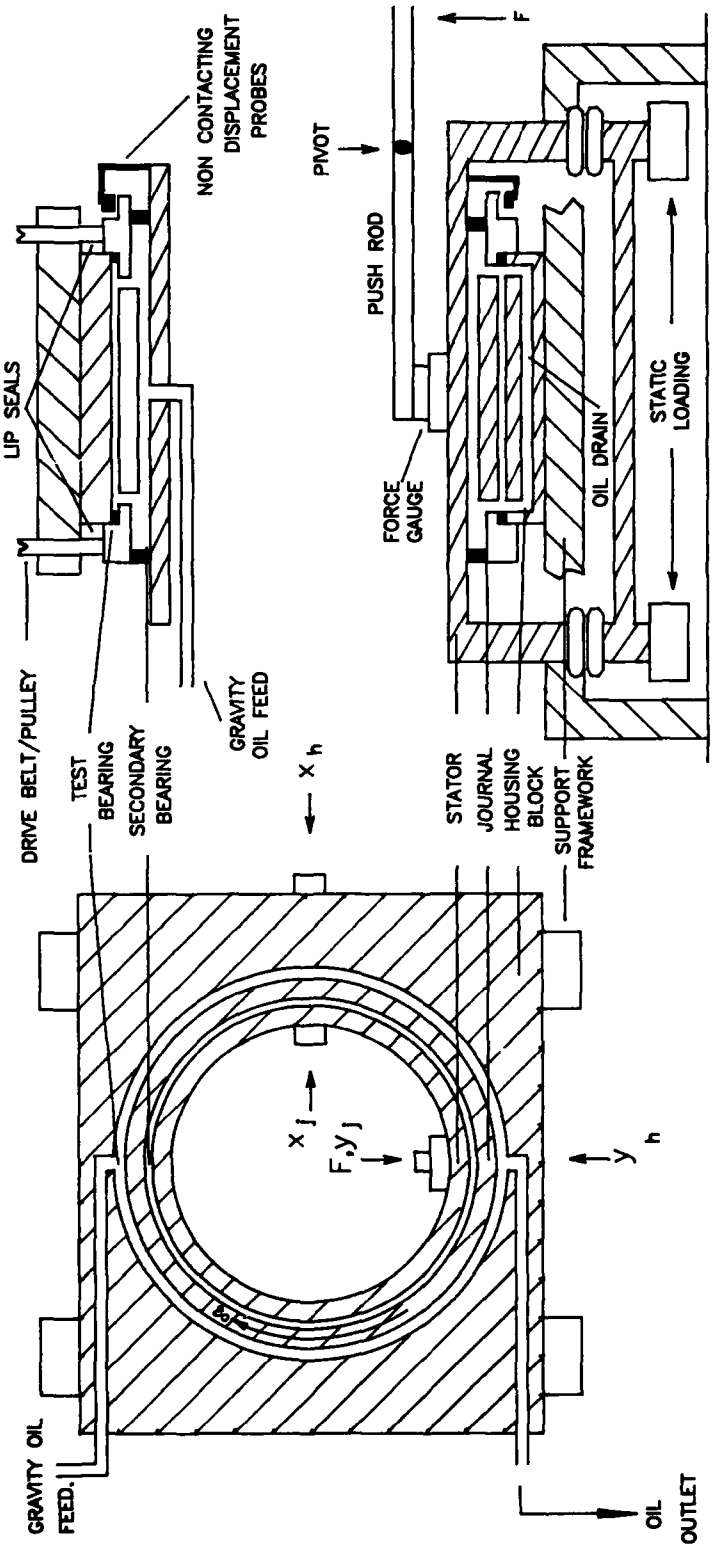

FIG 2. BEARING TEST RIG (NOT TO SCALE).

PLATE 1. BEARING TEST RIG - END VIEW

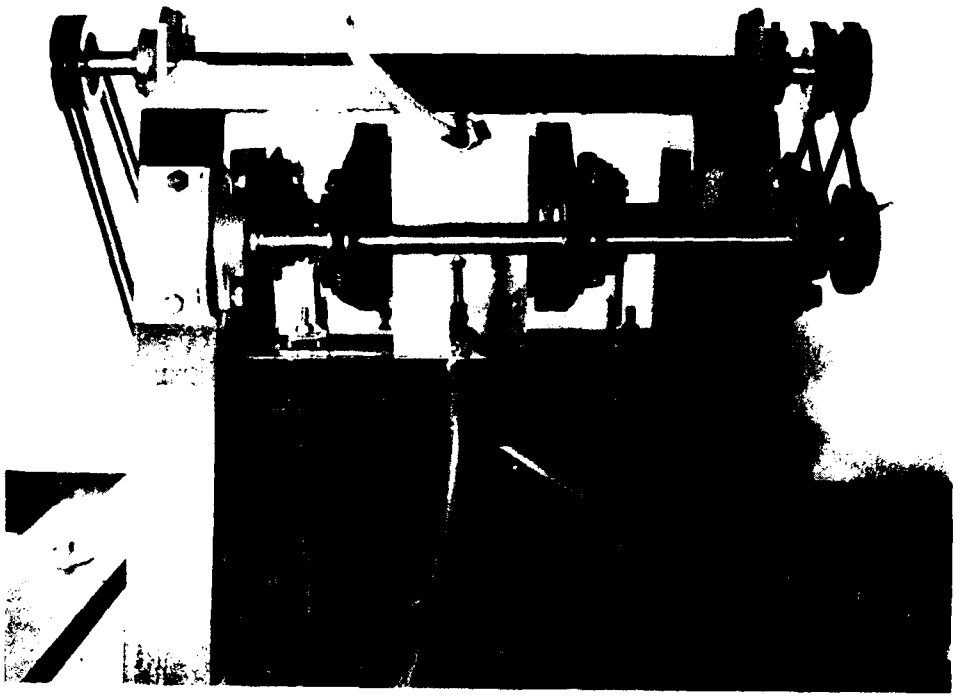

PLATE 2. BEARING TEST RIG - SIDE VIEW

5. INSTRUMENTATION AND ANALYSIS

The measurement chain is shown schematically in Figure 3. The swept sine wave technique was used for the transfer function measurements in order to eliminate extraneous non-linear effects. The analyser was a Solatron 1250 Frequency Response Analyser under the control of a Tetronix 4051 computer. Inertance data were plotted on line and stored to cassette. A Genrad 2508 Signal Analysis System was used to monitor the force and acceleration signals (ISAP software); this analyser was also used for the modulation investigation.

A steady input force of around 10N (which could be increased to a maximum of around 30N) was used when forcing on the housing; the push rod to the housing caused a resonance at around 2800Hz, but this was outside the frequency range of interest. When forcing on the journal a compressor was required to keep the input force at a steady level of up to around 20N; above 500Hz the compressor was no longer able to control the system and the force level rapidly fell (passing through a resonance at around 800Hz due to the lever system) to around 1N at 1000Hz.

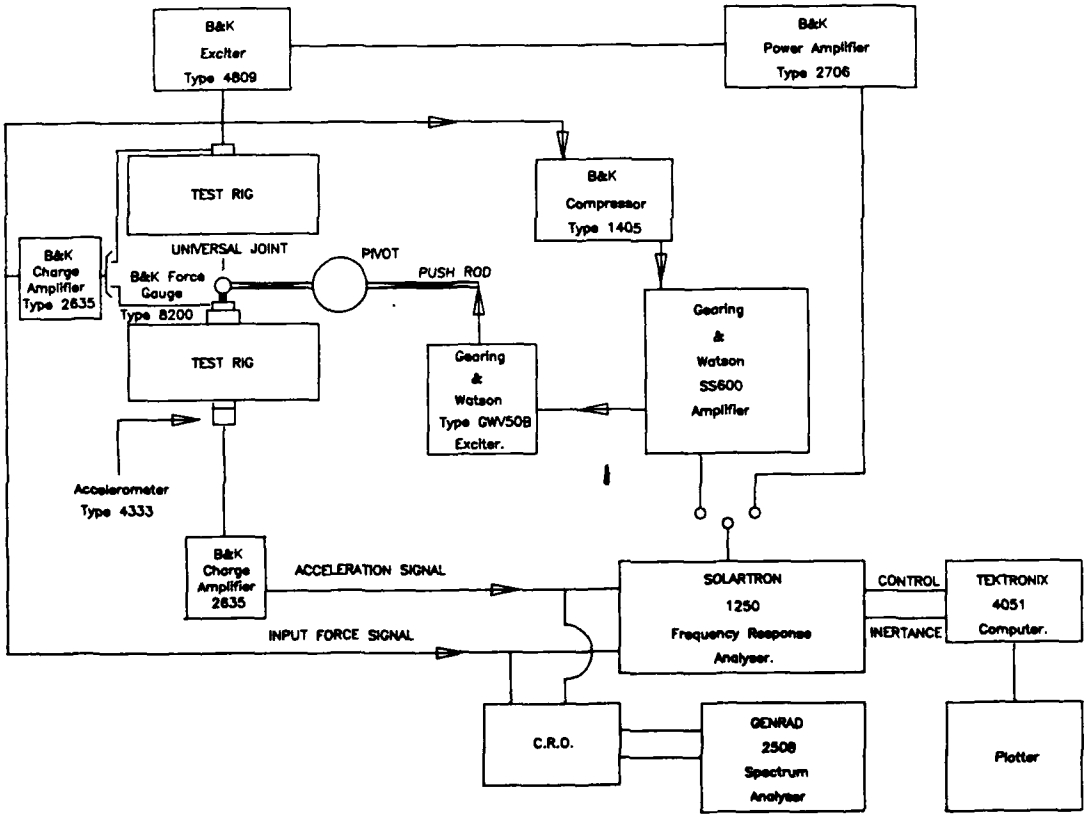

FIG 3. MEASUREMENT CHAIN

6. STRUCTURAL PROPERTIES OF STATIC TEST RIG.

Transfer function measurements were made on the test rig at various stages of assembly in order to characterise the dynamic behaviour and establish any limitations in its range of application.

For these tests the rig was exited at a point centred on the top of the housing using an input force of around 5N; the transfer functions to several representative points were measured for frequencies between 10Hz and 10kHz.

In addition, a modal analysis was performed on the assembled rig using Modal Plus software on the Genrad 2508 Signal Analysis System. In this case the input force (white noise with low and high frequency components filtered out) was applied off-centre on the top of the housing to avoid excitation at a nodal point and the triaxial responses were measured near the corners of the housing.

The point inertance at both excitation points are shown in Figure 4 for the fully assembled rig. The resonance at 114Hz is due to the rigid body motion of the rig in the vertical direction. Below this resonance the inertance corresponds to the vertical housing stiffness measured as $k = 3.2 \times 10^7$ Nm^{-1} and hence the stiff housing approximation applies. Above the resonance the inertance is determined by the combined mass of the block, journal and stator (but not the isolated static load) up to around 2kHz and hence the massive housing approximation applies.

It is worth noting that a resonance at √(housing stiffness / journal mass) predicted using the stiff housing approximation will never be observed in the real system since this prediction assumed the housing mass could be neglected. In the true system the frequency is shifted to √(system stiffness / system mass) and corresponds to the resonance at 114Hz.

The housing loses its rigidity at around 4kHz where the first flexing resonance of the housing block occurs. This puts an upper limit to the useful range of measurements.

Several lesser resonances were identified which are not all apparent in Figure 4 and are not expected to affect the investigation; these are summarised in Table 2. Using the lateral resonance at 67Hz the lateral housing stiffness was estimated as 1.2×10^{-7} Nm^{-1} .

It was concluded from these preliminary measurements that the test rig was suitable for assessing the validity of the theory in the frequency ranges 20Hz to 100Hz (stiff housing approximation) and 200Hz to 2000Hz (massive housing approximation). The low frequency region (below 20Hz) was limited by noise due to difficulty in applying sufficient force at these low frequencies.

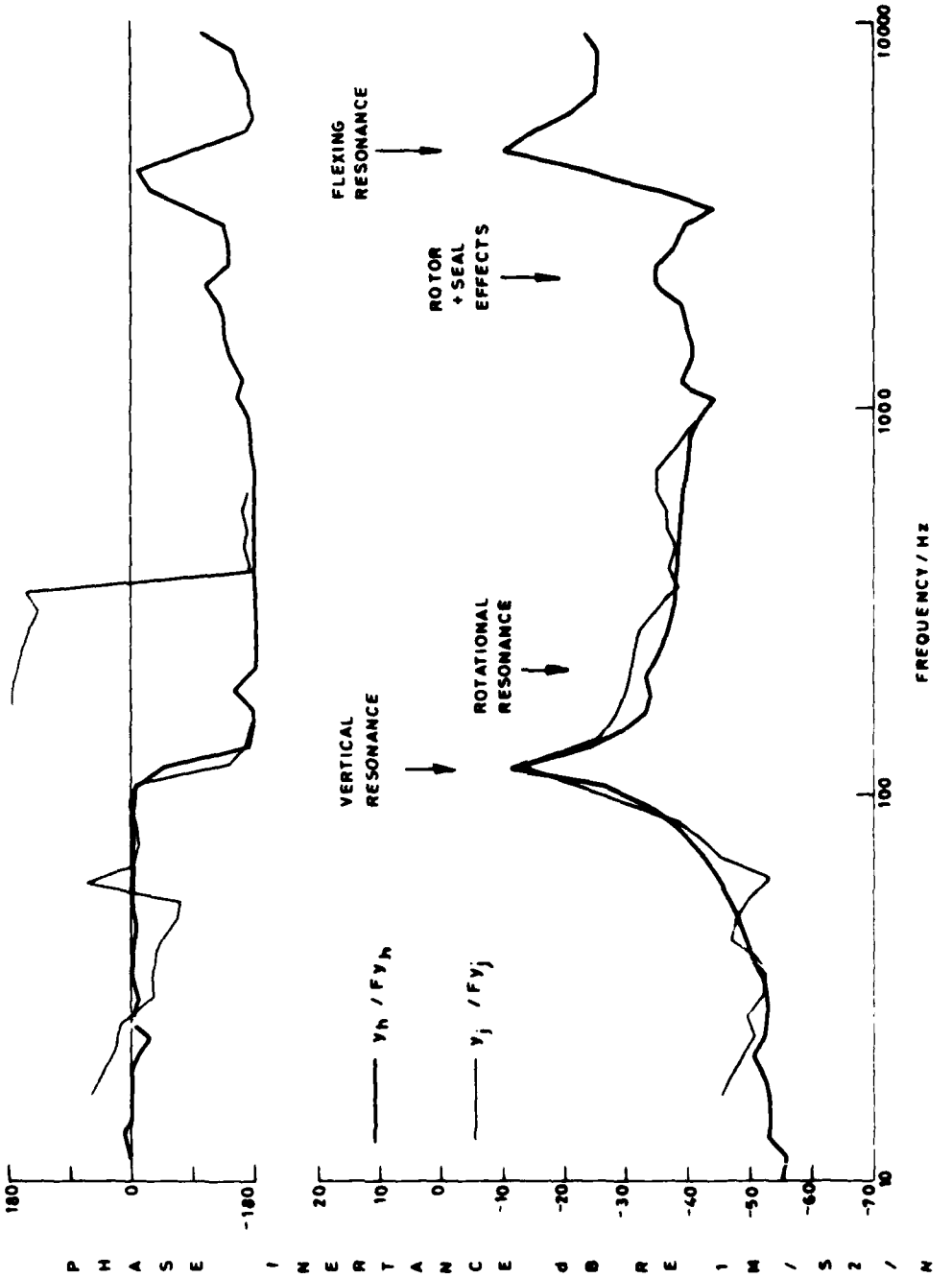

FIG. 4 POINT INERTANCES ON BEARING TEST RIG

TABLE 2. BEARING TEST RIG STRUCTURAL RESONANCES.

FREQUENCY Hz	SOURCE
67	Transverse translation
114	Vertical translation
177	Rotation in yz plane
191	
306	Rotation in xz plane
4300	Flexing

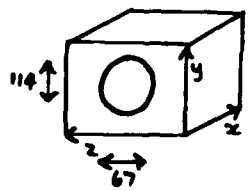

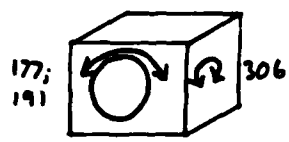

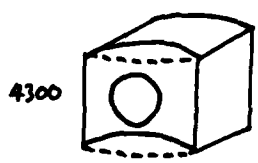

Additional effects:

34 (22;15)	Isolating mount resonance with 12kg (32;62kg) mass loading
950	Stator resonance - heavily damped on introduction of oil
2000 - 2500	Resonances associated with rotor and seals - heavily damped on introduction of oil.

7. BEARING PARAMETERS.

The test rig was run at shaft rates from 5Hz to 25Hz. The temperature measured at the oil outlet increased rapidly initially until reaching a "plateau" region where it continued to increase slowly but without stabilising completely within the time for which the rig could be run. Transfer function measurements were performed while the temperature was on this "plateau" region and the oil temperatures at the inlet and outlet were recorded both at the start and finish of the runs. The mean temperatures recorded over all runs are shown to the nearest degree in Table 3 for runs at 5, 10 and 20 Hz together with the associated standard deviations. The effective temperatures within the bearing were estimated (section 8.3 of [13]) using

$$T_{eff} = T_{inlet} + 1/2\,(T_{outlet} - T_{inlet})$$

The kinematic viscosities of the oils were determined from the effective temperatures using Figure 5 (taken from [12]) and hence the absolute viscosities were determined using the mean measured densities (Table 3).

The clearance of the test bearing was estimated from the oil flow rate at the inlet using the method recommended by Cameron [13, chapter 7] - see Appendix 2. The component from the inner bearing was eliminated for these measurements by clipping the supply to this bearing after stopping the rotor and the resulting flow rates are shown in Figure 6 as functions of the temperature at the oil inlet. Estimates for the clearance are shown in Figure 7 and show similar results for both oils as required; The "eye-average" line drawn through these results was taken as the standard curve. Unfortunately, however, since the design clearance is 0.5mm at room temperature, it would seem that the predictions are too large by a factor of 2. Although this factor could not be accounted for, the clearances which are listed in Table 3 for the operating rig have been renormalised on the assumption that the design specification was met. The agreement obtained between measured and predicted transfer functions (Sections 8 and 9) seems to justify this renormalisation.

The eccentricity ratio was estimated with the aid of Figure 8 by equating the static load F_0 to the steady oil film force:

$$-F_0 = \frac{12\pi\,\mu R^3 L\Omega m_0}{c^2(2+n_0^2)(1-n_0^2)^{1/2}} \qquad \text{Eq I.19a of [4]}$$

$$= \frac{A\Omega m_0}{(2+n_0^2)(1-n_0^2)^{1/2}} \simeq K\epsilon_0$$

Having established the bearing parameters under different running conditions, values could be estimated for the oil film stiffness and damping parameters. The short 360° bearing approximation was used since the bearing had a L/D ratio of unity and was fed through a central hole and drained at the ends; This meant an axial flow was likely to be dominant. The estimates for low eccentricity bearings are summarised in Table 3 while the estimates shown in Figure 9 include the effects of eccentricity; The stiffness coefficients are of the order of $10^7 Nm^{-1}$ when using OMD 113 oil and $10^6 Nm^{-1}$ when using OM 13 oil. Thus in the former case the bearing stiffness is estimated to be of the order of that of the housing ($K \simeq k$) while for the latter case the housing is more stiff ($K < k$).

It should be noted that the shaft rate dependance of the bearing damping coefficient is due to the reductions in the viscosity and clearance as a result of the increase in temperature at higher shaft rates . This same dependance is reflected in the stiffness coefficients and modifies the direct dependance on the shaft rate.

Table 3 indicates the effect of bearing temperature variability on the stiffness and damping parameters (for low eccentricity) at the specified shaft rates by showing the estimated values corresponding to temperatures at one standard deviation below and above the mean. The results for the OMD113 oil are more variable (up to 40% at worst) than those for the OM13 oil (up to 10%) due to the wider spread of operating temperatures at given shaft rates. However, this variability is not reflected in the eventual transfer function predictions since these are governed in the case of the OMD113 oil by the housing stiffness (see section 8).

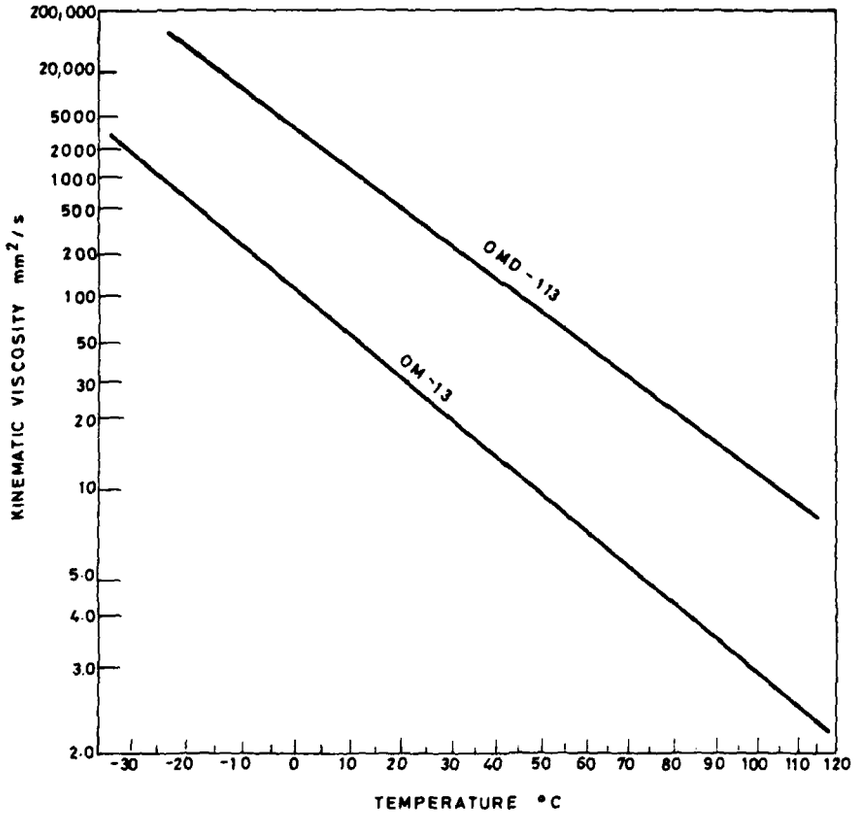

FIG. 5 OIL VISCOSITY [12]

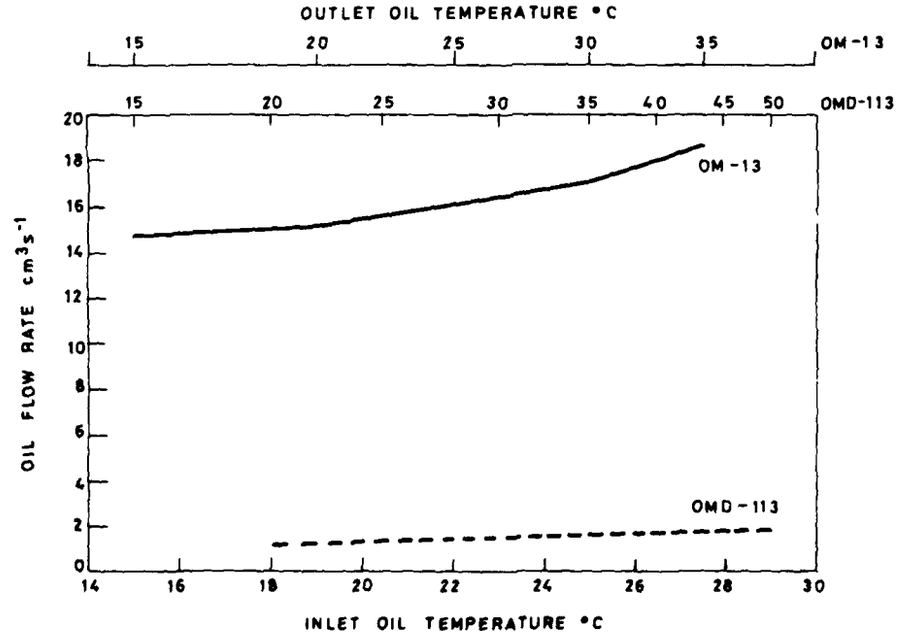

FIG. 6 MEASURED OIL FLOW RATE AS A FUNCTION OF INLET TEMPERATURE

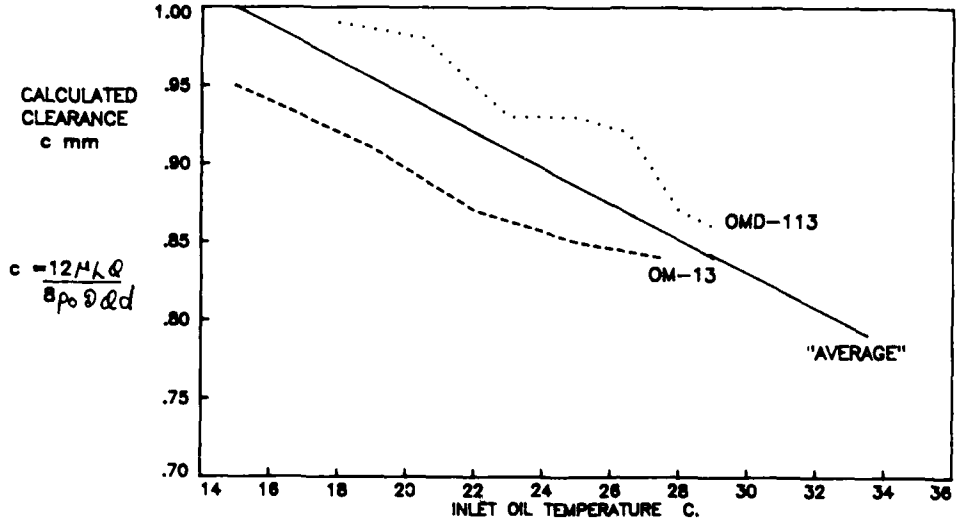

FIG 7. CLEARANCE ESTIMATES.

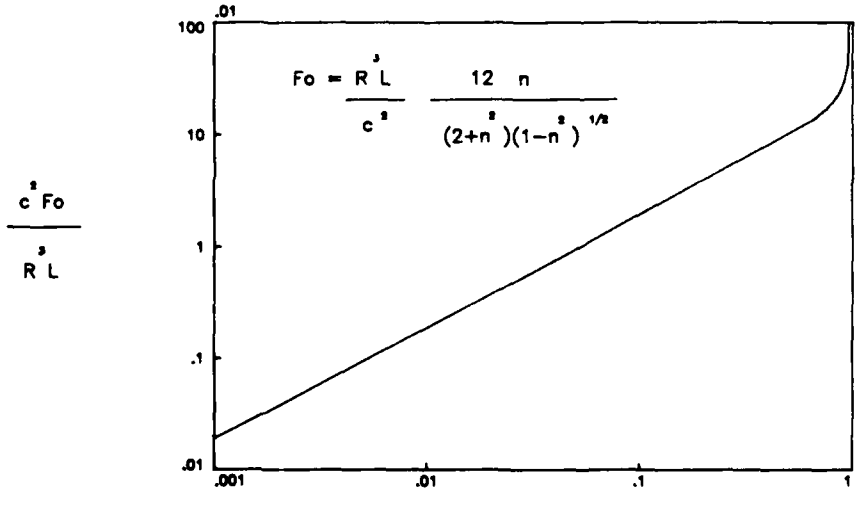

FIG 8. GRAPHICAL AID TO DETERMINING ECCENTRICITY RATIO.

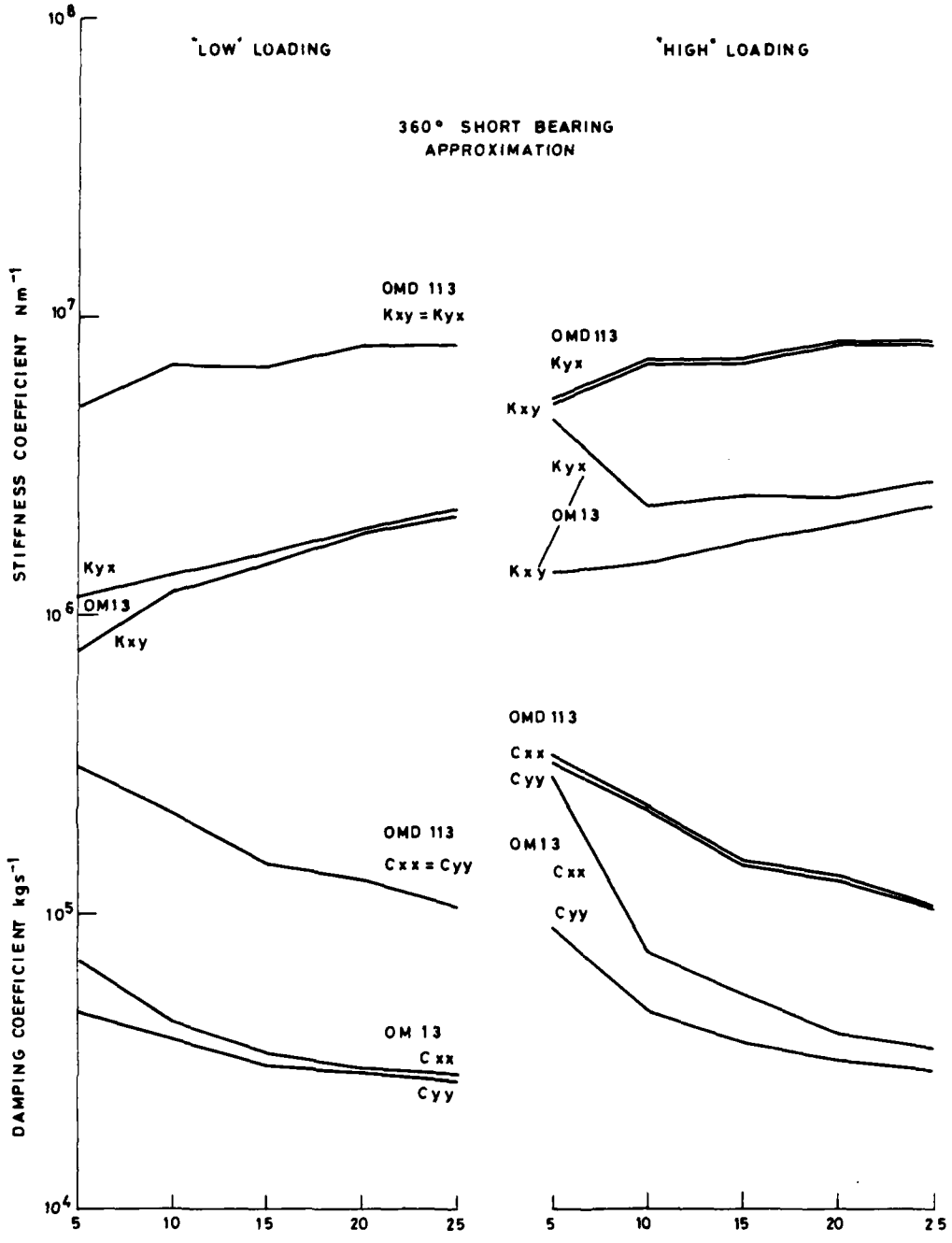

FIG. 9 STIFFNESS AND DAMPING COEFFICIENTS OF TEST BEARING (SHORT 360° BEARING APPROXIMATION)

TABLE 3. TEST BEARING PARAMETERS

Oil type		OMD 113 (ρ=820kgm^{-1})			OM 13 (ρ=830kgm^{-1})		
Shaft rate f Hz		5	10	20	5	10	20
Angular frequency Ω Hz		31	63	126	31	63	126
Temperature at inlet: Mean (SD) T_{in} °C		24(6)	27(4)	30(3)	20(2)	21(2)	27(3)
Temperature at outlet: Mean (SD) T_{out} °C		33(6)	41(5)	55(6)	21(3)	24(2)	34(4)
Effective bearing temperature T_{eff} °C		31	38	50	21	23	33
Effective kinematic viscosity ν m^2s^{-1}		2.2×10^{-4}	1.4×10^{-4}	7.5×10^{-5}	3.0×10^{-5}	2.6×10^{-5}	1.7×10^{-5}
Absolute viscosity $\mu = \nu\rho$ $kgm^{-1}s^{-1}$		.18	.11	.062	.025	.022	.014
Clearance c mm		.45	.43	.42	.47	.46	.43
$FL = \frac{F_0c^2}{R^3\mu L\Omega}$	F_0 = 320N	.92	.69	.58	7.2	3.9	2.7
	F_0 = 820N (OMD113) = 620N (OM13)	2.4	1.8	1.5	14	7.6	5.1
Eccentricity ratio	F_0 = 320N	.048	.036	.031	.38	.21	.14
	F_0 = 820N (OMD113) 620N (OM13)	.13	.098	.080	.66	.40	.27
$\pi B = \frac{R L^3 \mu \pi}{c^2}$ $kgms^{-1}$		140	93.3	53.3	17.7	16.3	12.0
* Bearing stiffness (F_0 = 320N) $K = \frac{B\pi\Omega}{2c}$ Nm^{-1}		5.0×10^6 (.63,.43)	6.7×10^6 (.97,.63)	8.3×10^6 (1.0,.83)	6.0×10^5 (.63,.57)	1.1×10^6 (1.1,1.1)	1.8×10^6 (1.9,1.6)
* Bearing Damping (F_0 = 320N) $C = \frac{B\pi}{c}$ kgs^{-1}		3.1×10^5 (4.0,2.8)	2.2×10^5 (3.1,2.0)	1.3×10^5 (3.1,1.3)	3.7×10^4 (4.0,3.7)	3.7×10^4 (3.7,3.3)	2.8×10^4 (3.0,2.5)
$m_j\Omega^2$ kgs^{-2}		2.0×10^4	7.9×10^4	3.2×10^5	2.0×10^4	7.9×10^4	3.2×10^5

* The terms in brackets indicate the values of K and C evaluated at T(mean-1SD) and T(mean+1SD)

8. TRANSFER FUNCTION PREDICTIONS

Expressions for the bearing transfer functions were derived in Part 1 and are summarised in Appendix 3. Although the mathematical expressions derived are somewhat complex, the theory can be interpreted in a simple manner with the aid of Figure 10. When the oil film damping coefficient is very high (so that the bearing is very stiff) the bearing is rigid to vibration and the system behaves as a lumped mass on a spring (Figure 10a) with a resonance at

√ (housing stiffness / combined mass of housing and journal)

Below the resonance the inertances are determined by the housing stiffness

$$\frac{\ddot{y}_j}{Fy_j} = \frac{\ddot{y}_h}{Fy_h} = \frac{\ddot{y}_j}{Fy_h} = \frac{\ddot{y}_h}{Fy_j} = \frac{-\omega^2}{k_h} \quad \text{(From A3.9 and A3.10)}$$

While above the resonance they are given by the combined mass

$$\frac{\ddot{y}_j}{Fy_j} = \frac{\ddot{y}_h}{Fy_h} = \frac{\ddot{y}_j}{Fy_h} = \frac{\ddot{y}_h}{Fy_j} = \frac{1}{(m_j + m_h)} \quad \text{(From A3.15 and A3.16)}$$

At very high frequencies the journal and housing decouple (Figure 10b) so that the point inertances are given by the individual masses while the transfer inertances, which are reciprocal, begin to fall off with frequency and are determined by the oil film damping.

$$\frac{\ddot{y}_j}{F_j} = \frac{-1}{m_j} \qquad \frac{\ddot{y}_h}{F_h} = \frac{-1}{m_h}$$

$$\frac{\ddot{y}_j}{F_h} = \frac{\ddot{y}_h}{F_j} = \frac{C}{m_j m_h \omega}$$

Thus at high frequencies the bearing becomes elastic if the oil film damping coefficient is reduced (Figure 10c) then the frequency at which the system decouples is decreased so that the bearing becomes elastic over a wider frequency range. Some decoupling also occurs at lower frequencies,particularly in the region of the oil whirl resonance (not shown) which mostly affects the journal. Thus, if the oil film damping is very low the bearing will be elastic over most of the frequency range except in the region of the system resonance.

Figure 11 shows the behaviour predicted from the full equations (A3.1 and A3.2) for both the high and low viscosity oils with the rig running at 10Hz under 'low' loading (low eccentricity). The transfer functions have been converted to inertances for direct comparison with experiment by multiplying by the square of the forcing frequency.

The predicted cross inertances are also shown in Figure 11 and are predicted to be some 50dB down on the point and transfer inertances. These show two resonances corresponding to the vertical and transverse vibration

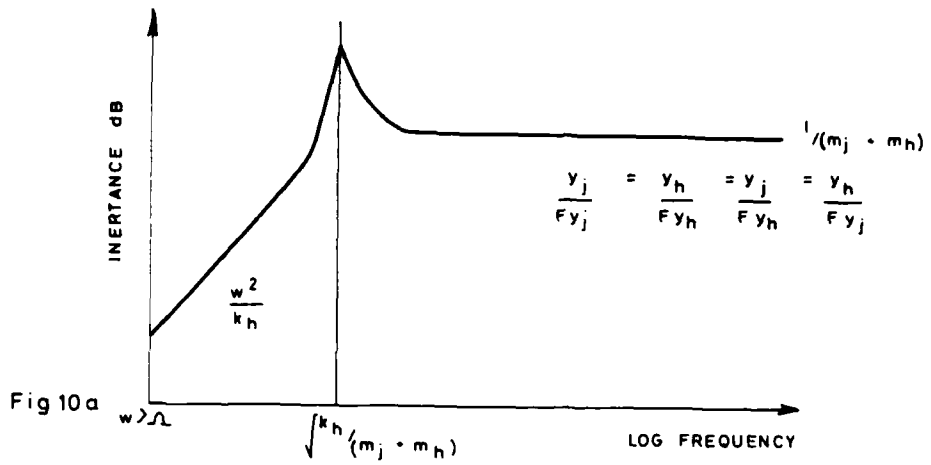

Fig 10a

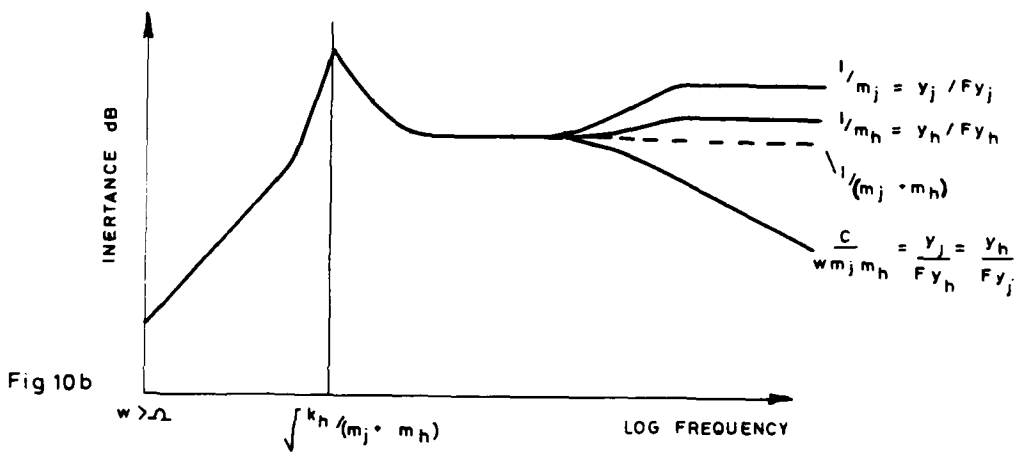

Fig 10b

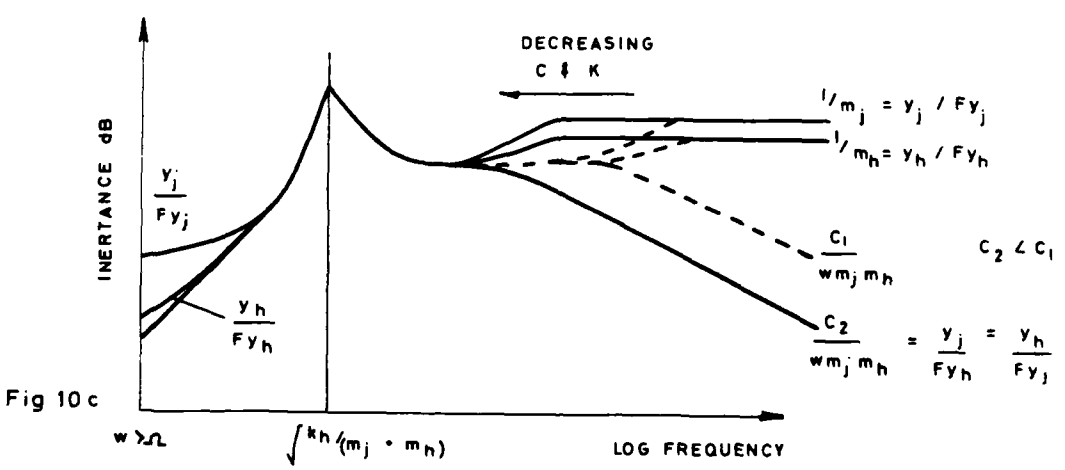

Fig 10c

FIG. 10 INTERPRETATATION OF THEORY

FIG 11 PREDICTED INERTANCES AT 10Hz UNDER LOW LOADING (LOW ECCENTRICITY) 360° 'SHORT' BEARING

modes. In this case the bearing is no longer predicted to be rigid. Refering to equation A3.17 it can be seen that the differences are due to the contributions from the mass terms:

$$\frac{\ddot{x}_j}{F_{yj}} \alpha \frac{1}{m_j^2} \quad ; \quad \frac{\ddot{x}_h}{F_{yj}} \alpha \frac{\ddot{x}_j}{F_{yh}} \alpha \frac{1}{m_h m_j} \quad ; \quad \frac{\ddot{x}_h}{F_{yh}} \alpha \frac{1}{m_h^2}$$

and inserting values for m_j and m_h gives the 7dB difference predicted between the levels in Figure 11.

Shaft rate dependence

As the shaft rate of the test rig increases, the damping coefficients decrease (Figure 9) so that the onset of decoupling above the system resonance occurs at successively lower frequencies (Figure 10). Thus, at a given frequency the point inertances will increase with increasing shaft rate until reaching the limiting value determined by the relevant mass. The transfer functions, however, will decrease. In the latter case the limiting value itself is determined by the bearing damping and this introduces a further decrease with shaft rate. These changes can be seen in figures 14 and 16 which show the inertances calculated for the test rig running at thre different shaft rates with the two different oils.

The cross inertances are directly related to the bearing stiffness and, at some frequencies, are proportional to the inverse square of the bearing damping (equations A3.8 and A3.17). They will therefore increase with shaft rate. Predictions for the test bearing are shown in figures 18 and 19.

Eccentricity and its effects on Reciprocity

The bearing stiffness and damping parrameters are dependent on the eccentricity (Table 3.1) and are no longer expected to be symmetric when the eccentricity is high enough to take effect. Figures 20 and 22 show the predicted effects of increasing the eccentricity. The example used is that of the test rig running at 5Hz with OM13 oil since table 3 shows this to be the case where the bearing is most eccentric. The eccentricity ratios assumed were .38 and .66, the values estimated for the rig under low and high loads respectively, and .98. The point and transfer inertances (Figure 20) are hardly affected until the eccentricity becomes very high. The transfer functions remain reciprocal.

The cross inertances are expected to decrease with increasing eccentricity . The reciprocal cross inertances are also shown in Figure 22 and indicate that with increasing eccentricity, reciprocity should cease to apply;this is due to the asymmetry of the bearing stiffness and damping matrices.

9 MEASURED LINEAR TRANSFER FUNCTIONS.

Linear transfer functions were obtained for both the OMD113 and OM13 oils with the rig running at 5, 10, 15, 20 and 25Hz and with the input forces applied in turn to the housing and journal.

Figure 12a and 12b show the inertances measured with the rig running at 10Hz. The point and transfer inertances are compared directly with the theoretical predictions in figures 13a and 13b.

Forcing Housing (Figure 13a)

Considering first the results obtained when forcing on the housing it can be seen that there is a very good agreement between the predicted and measured results. The bearing is rigid in the direction of the applied force up to around 500Hz when using the high viscosity oil while for the low viscosity oil the bearing is rigid only in the region of the resonance. As predicted the response is reduced on transmission across the bearing at frequencies above the resonance .

The peak observed at 200Hz is due to the rotational mode of the housing (table 2) which has been excited due to the unavoidable off-setting of the input force. This does not appear in the theoretical curves since the predictions are for a centralised force which would not excite this mode. The deviation from the predicted behaviour above about 200 Hz is due to the effects of other resonances seen also in the static point inertance (Figure 4, Table 2).

The cross inertances are extremely noisy. Peaks can be identified at around 70Hz (transverse mode), 120Hz (vertical mode) and 180Hz (rotational mode). Away from the 70Hz and 120Hz resonances the cross transfer functions were predicted to be exceptionally low. These predictions could not be validated as the measured results were very noisy. This noise was due to pick up from the transducer transverse sensitivity in addition to the noise of the running rig; there was also interference from other modes, such as the rotational modes. Although the effect of the bearing could not be isolated in these measurements, it must be very low, as predicted.

Forcing Journal (Figure 13b)

When forcing on the journal the results were very noisy up to about 70Hz and were affected by a resonance at 50Hz which was later found to be due to the effect of the static loading acting on the W mounts. Above 70Hz the driving force was sufficient to overcome the rig noise and so produce true inertance measurements.

A prominent resonance appeared at 220Hz in all measurements on the journal when forcing on the journal but this was not present on the housing. This resonance was found to be due to a very strong axial vibration of the stator on the inner bearing which only set in when the bearing was operative.

At higher frequencies (above 600Hz) the point inertance begins to increase with forcing frequency while the transfer inertance decreases and this is in qualitative agreement with the predictions.

The cross inertances are again inconsistent with those predicted due to noise and other effects.

Shaft Rate Effects

Figures 15 and 17 show the point and transfer inertances for OMD113 and OM13 oils respectively measured on the static rig and at varying shaft rates. The variations are small, as predicted, and the increase or decrease with shaft rate is in accordance with the theoretical predictions shown in Figures 14 and 16. The cross inertances were very noisy as already mentioned and it was therefore not possible to confirm the predictions made for these in Figures 18 and 19.

Eccentricity Effects

In order to increase the eccentricity of the running rig extra mass was added to the static load (an additional 50kg when running with OMD113 oil but only 30kg when running with OM13 oil since the rig became unstable with any higher load). Estimates for the increased eccentricities are shown in Table 3. The transfer function measurements were repeated. The point and transfer inertances showed little difference from the previous (low eccentricity) runs, the only difference being that the resonance attributed to axial shuffling shifted to a slightly lower frequency as did the low frequency resonance associated with the action of the static load on the ω mounts.

Figure 21 compares the inertances measured on the bearing under low and high loading with the rig running at 5Hz with OM13 oil. The variations which occur are consistent with theory but are insufficient for conclusive validation. Unfortunately the static load could not be further increased in order to further validate the high eccentricity effects as the bearing became unstable under additional loading.

The predicted decreases in the cross inertances could not be observed as these measurements were noise limited.

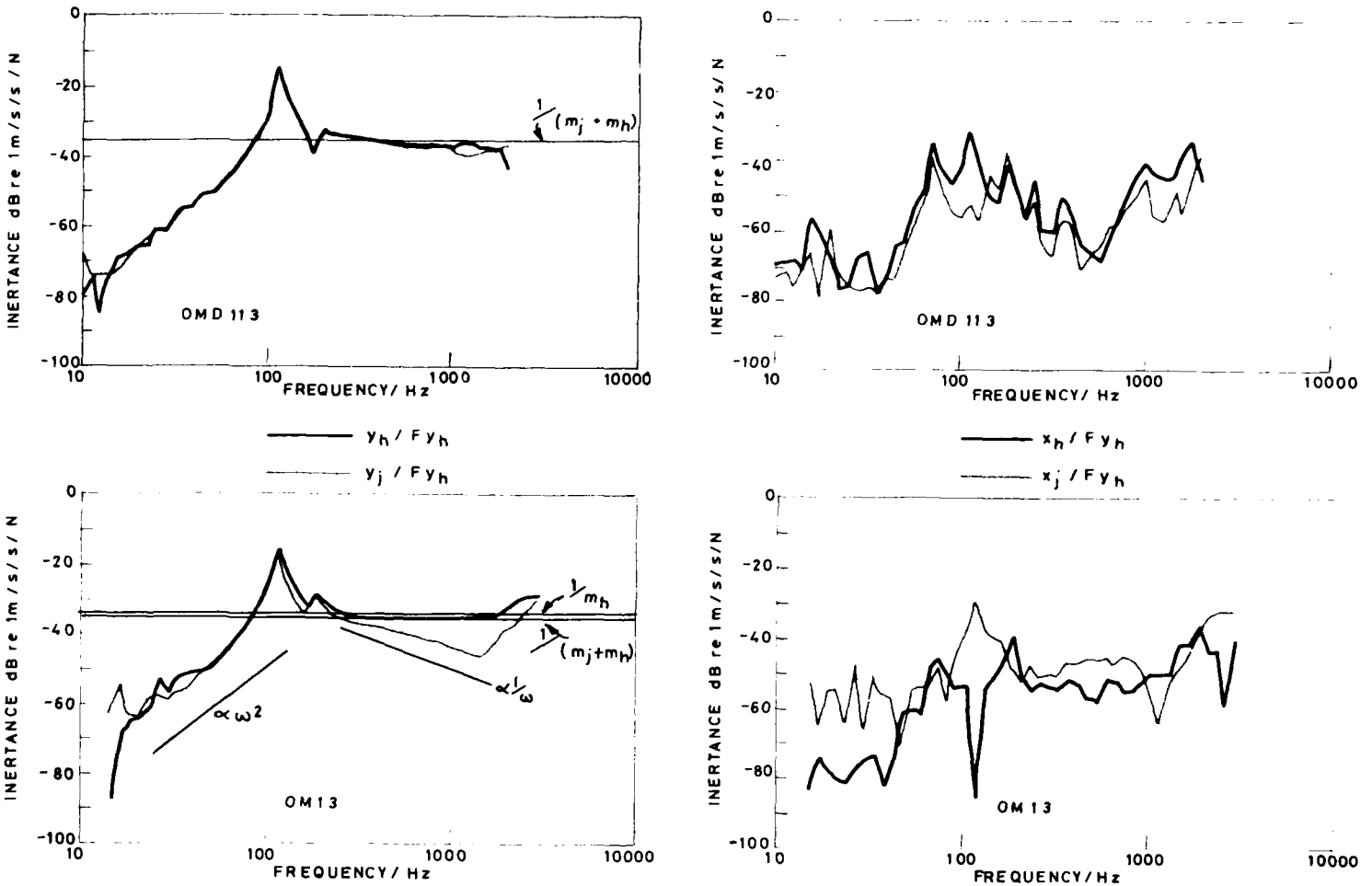

FIG. 12 a MEASURED INERTANCES AT 10Hz UNDER LOW LOADING (LOW ECCENTRICITY) FORCING HOUSING

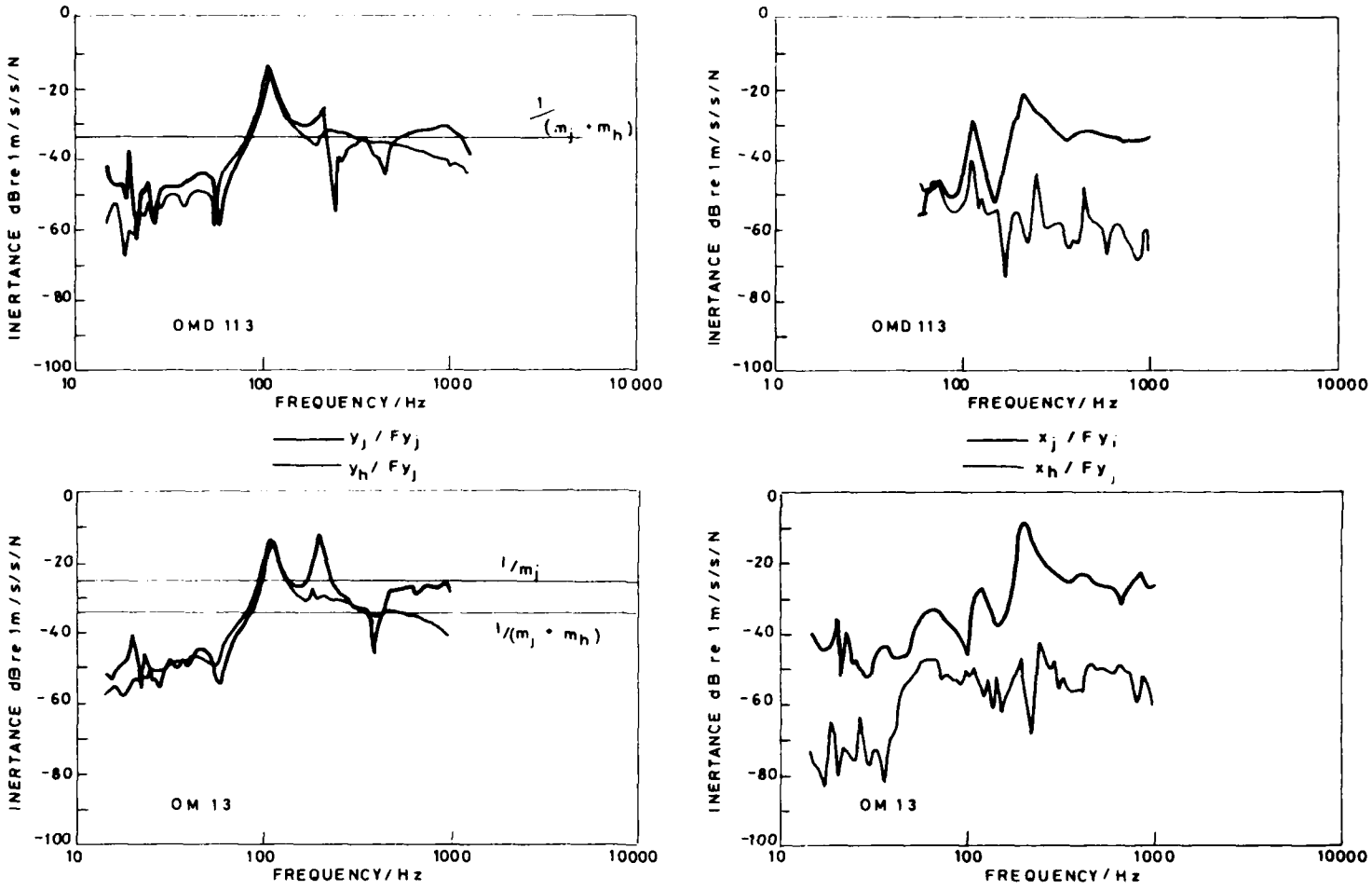

FIG. 12b MEASURED INERTANCES AT 10Hz UNDER LOW LOADING (LOW ECCENTRICITY) FORCING JOURNAL

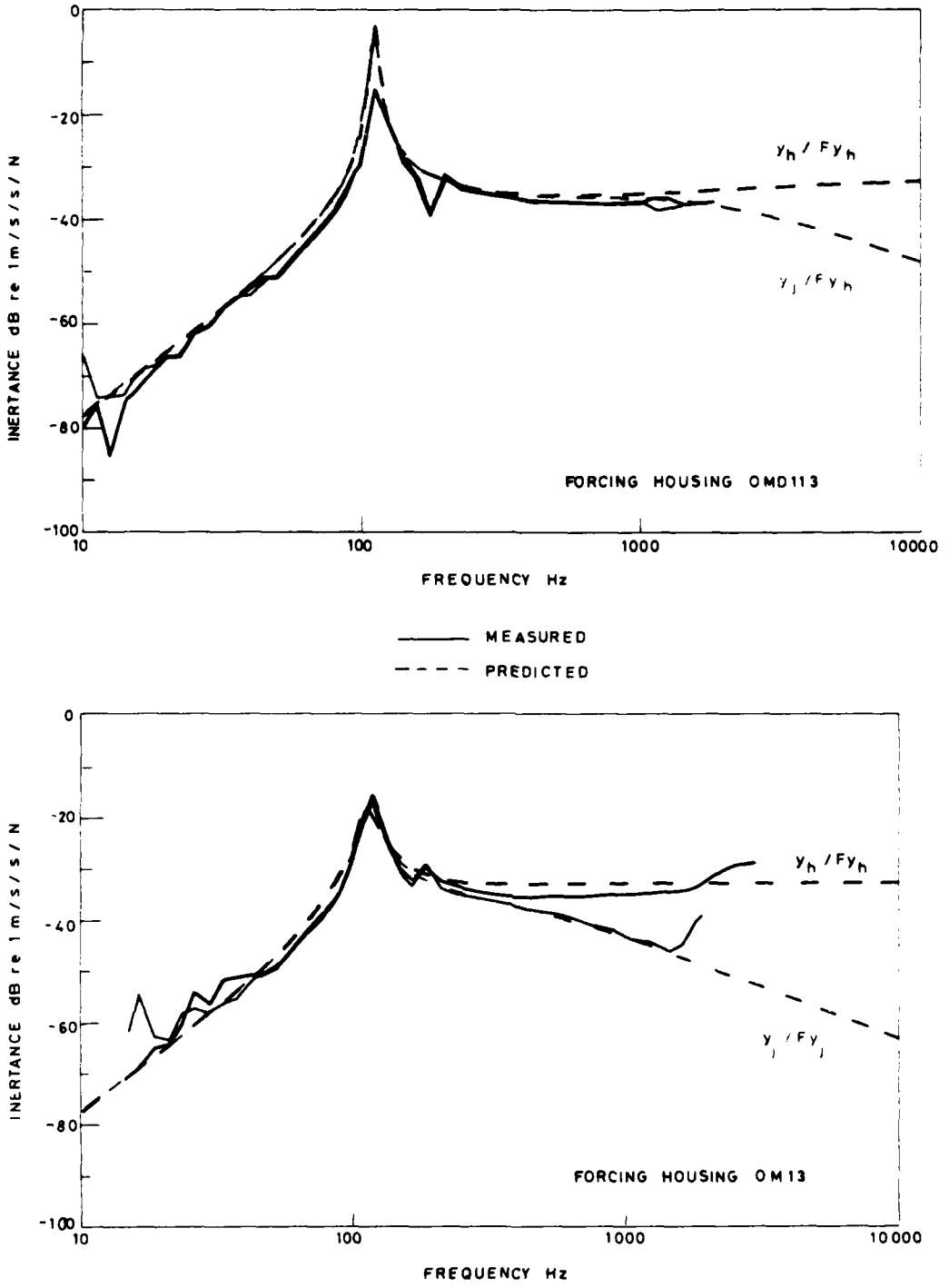

FIG. 13a COMPARISON OF MEASURED AND PREDICTED INERTANCES
10Hz SHAFT RATE, LOW LOADING

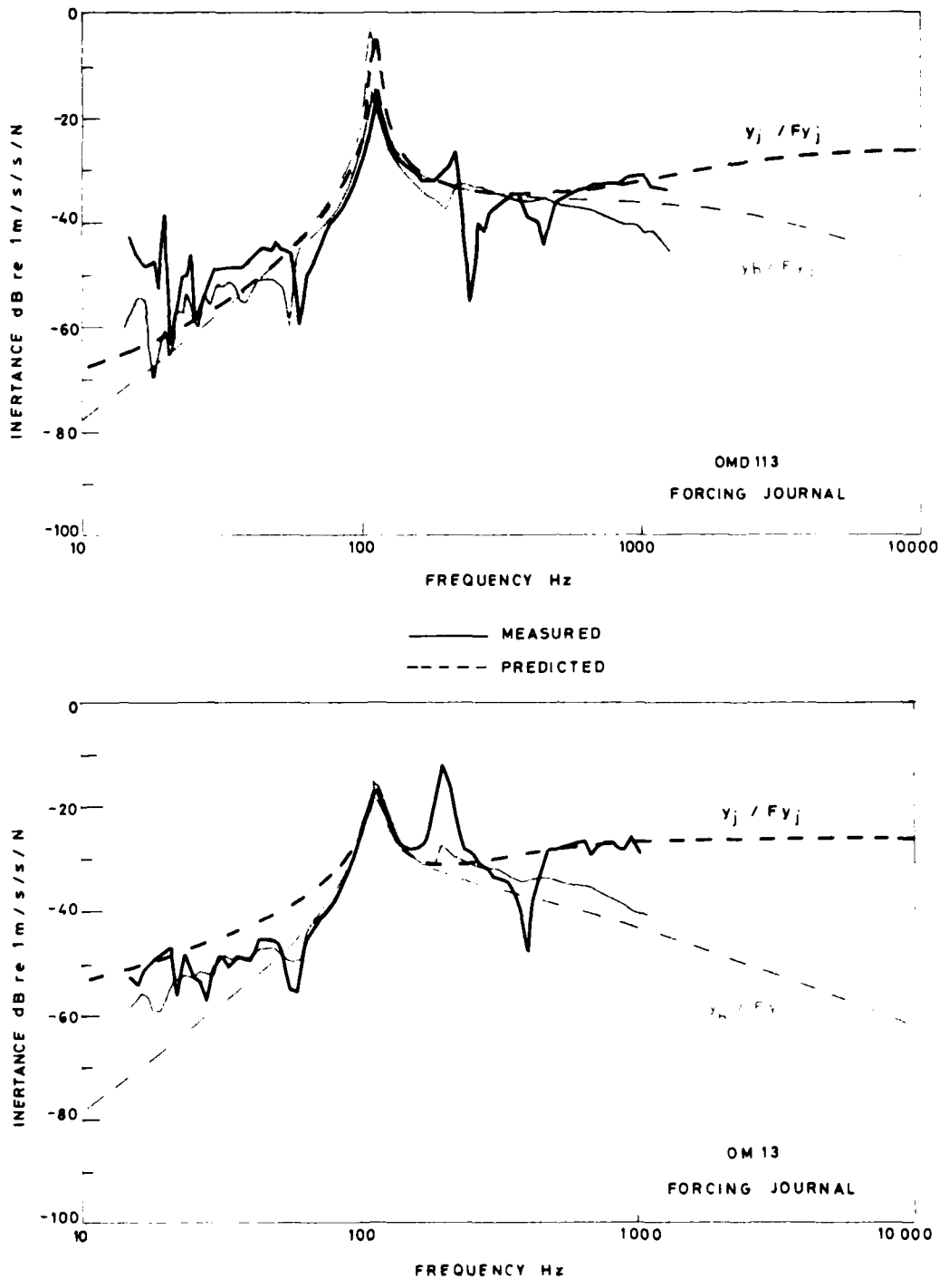

FIG 13b COMPARISON OF MEASURED AND PREDICTED INERTANCES
10Hz SHAFT RATE, LOW LOADING

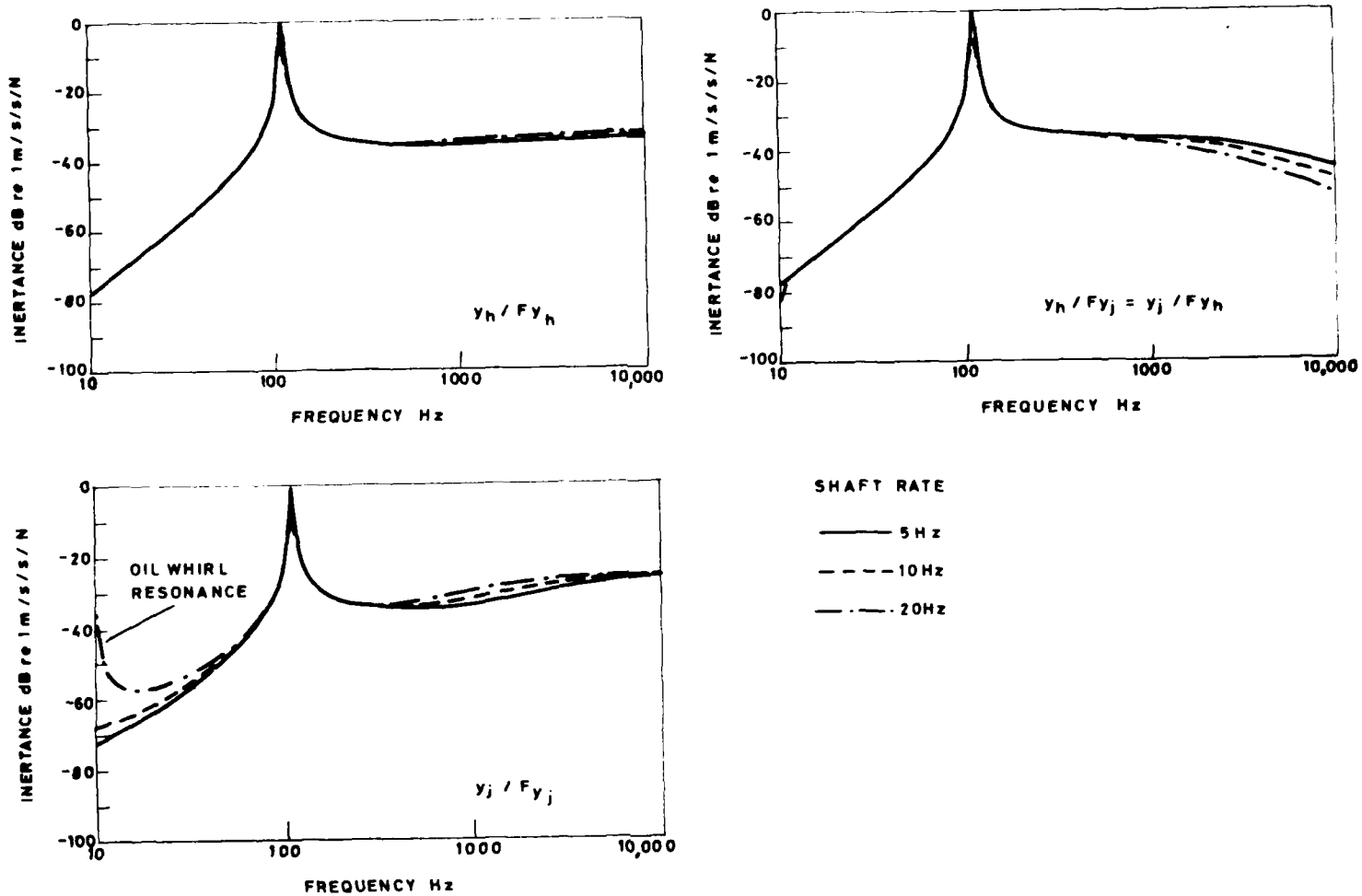

FIG. 14 PREDICTED POINT AND TRANSFER INERTANCES FOR OMD 113 OIL AT VARIOUS SHAFT RATES (LOW LOAD) 360° SHORT BEARING APPROXIMATION

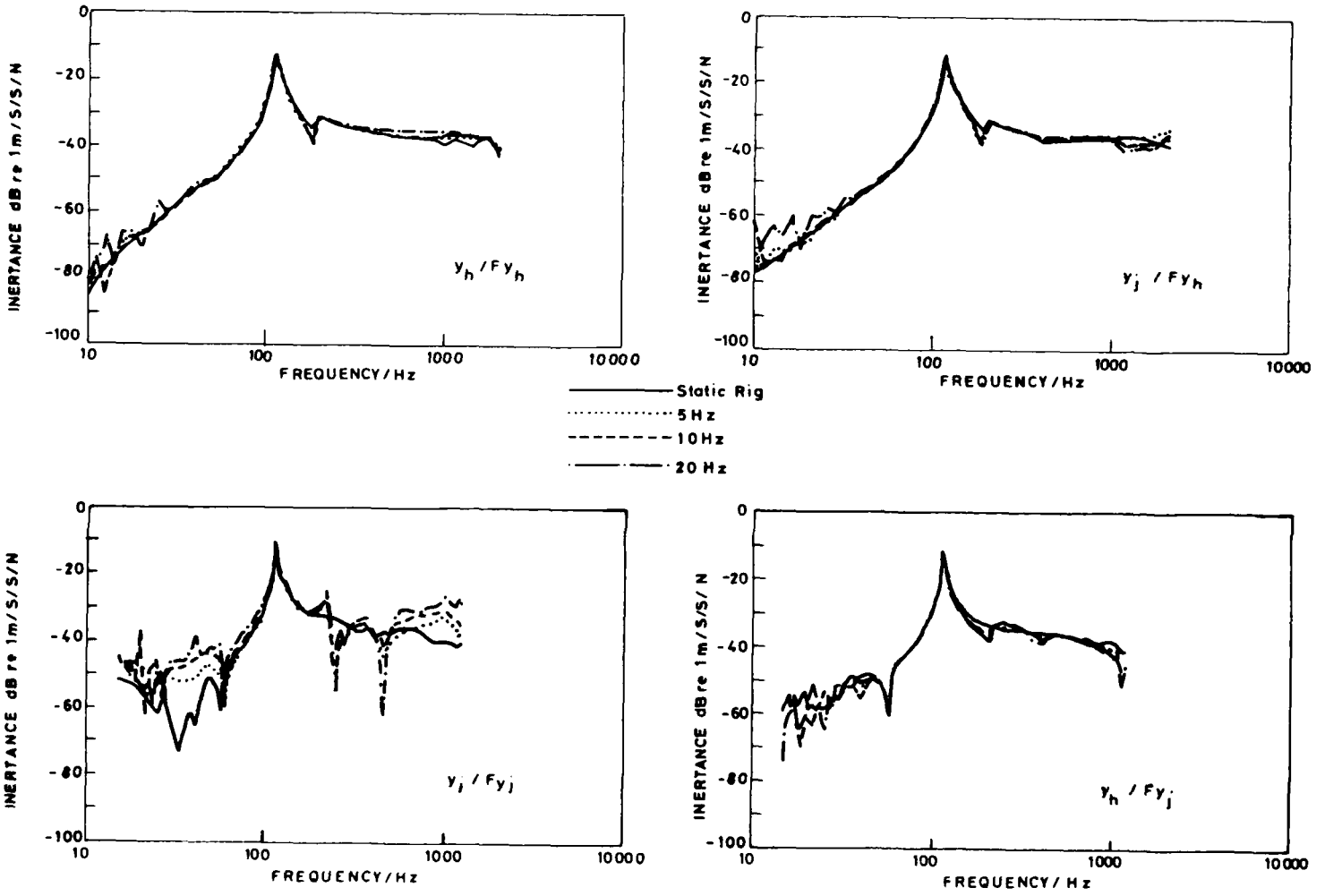

FIG. 15 MEASURED POINT AND TRANSFER INERTANCES FOR OMD113 OIL AT VARIOUS SHAFT RATES (LOW LOAD)

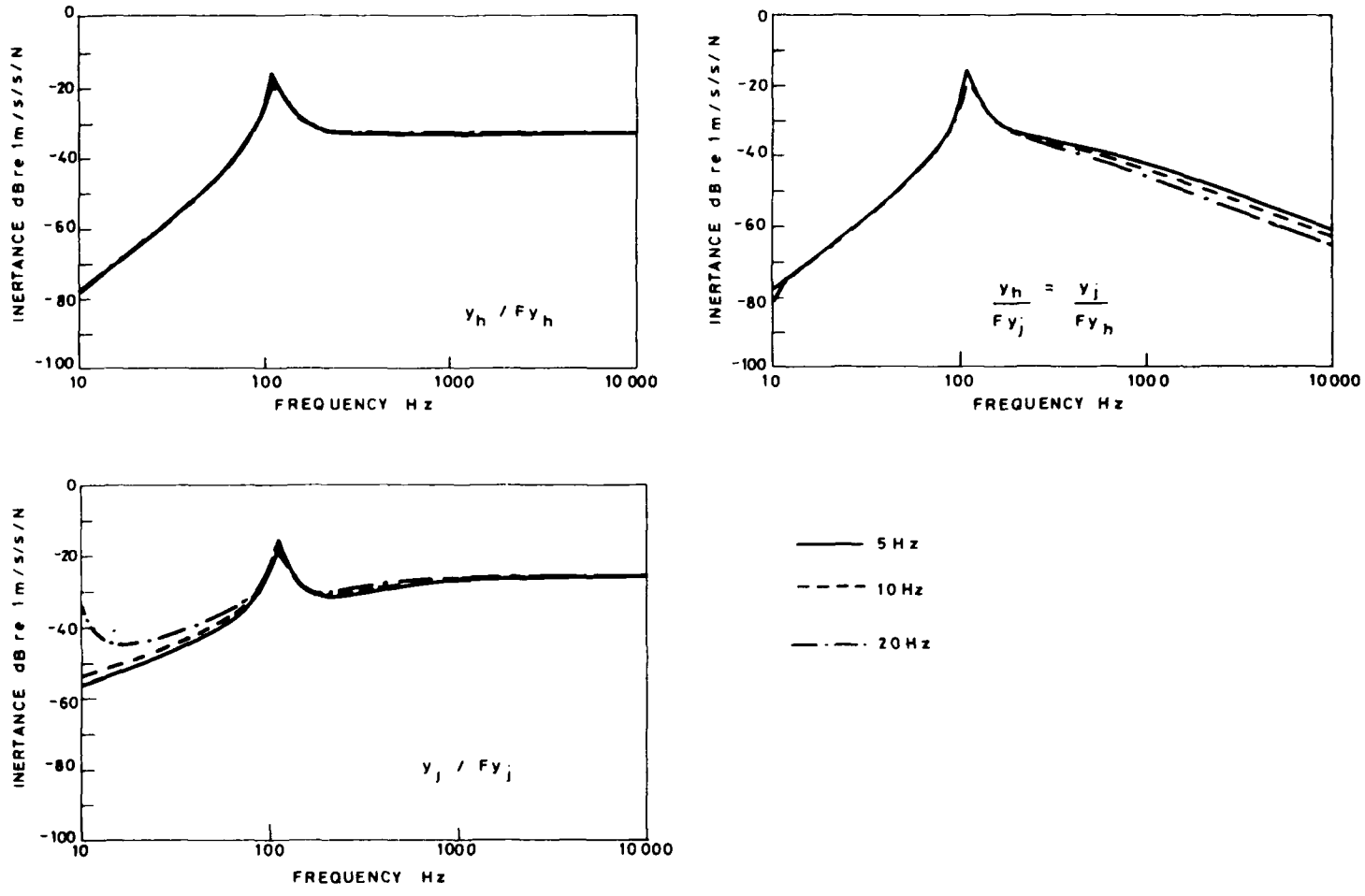

FIG 16 PREDICTED POINT AND TRANSFER INERTANCES FOR OM13 OIL AT VARIOUS SHAFT RATES (LOW LOAD) SHORT 360° BEARING APPROXIMATION

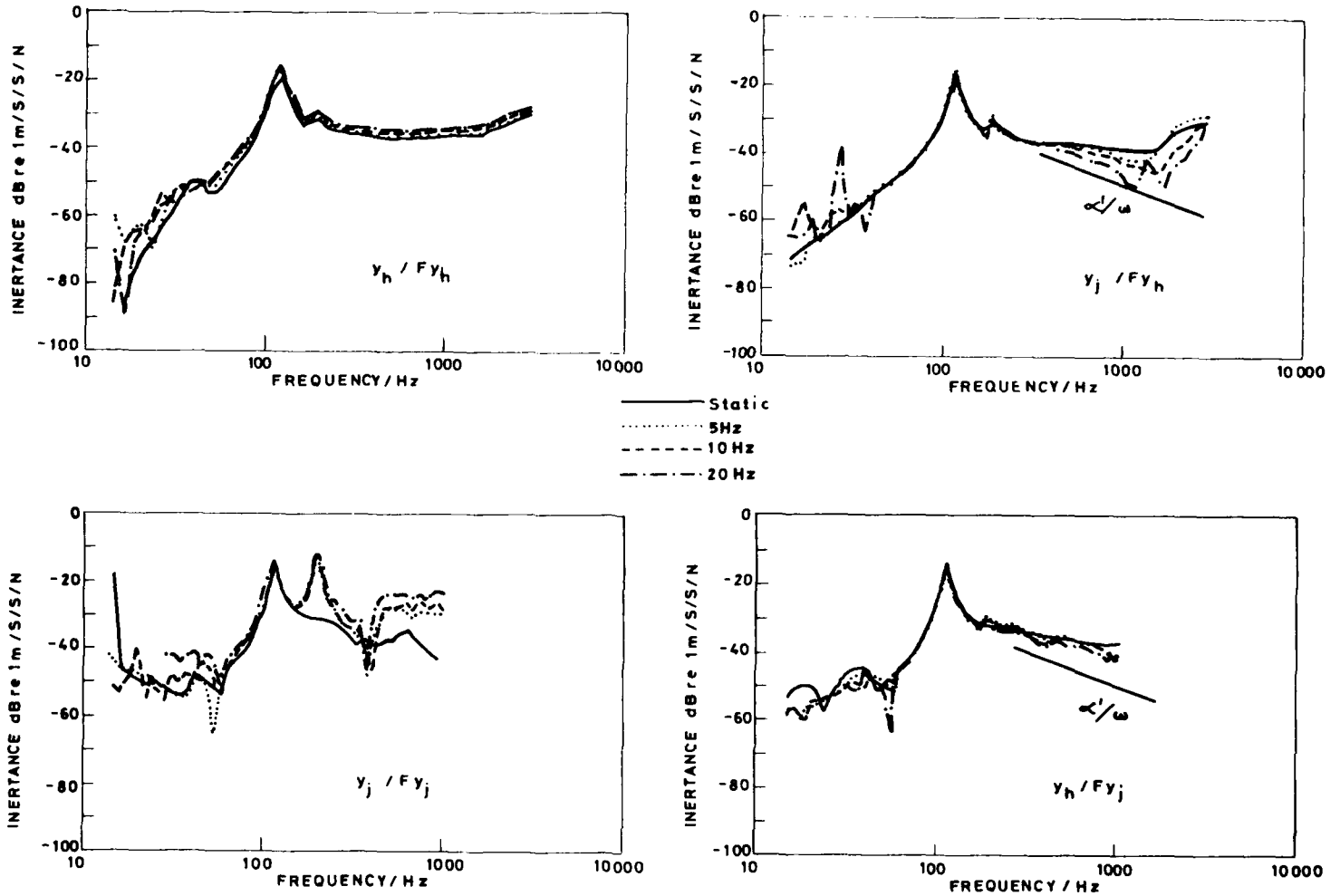

FIG 17 MEASURED POINT AND TRANSFER INERTANCES FOR OM13 OIL AT VARIOUS SHAFT RATES (LOW LOAD)

FIG. 18 PREDICTED CROSS INERTANCES FOR OMD 113 OIL AT VARIOUS SHAFT RATES - LOW LOAD - SHORT 360° BEARING

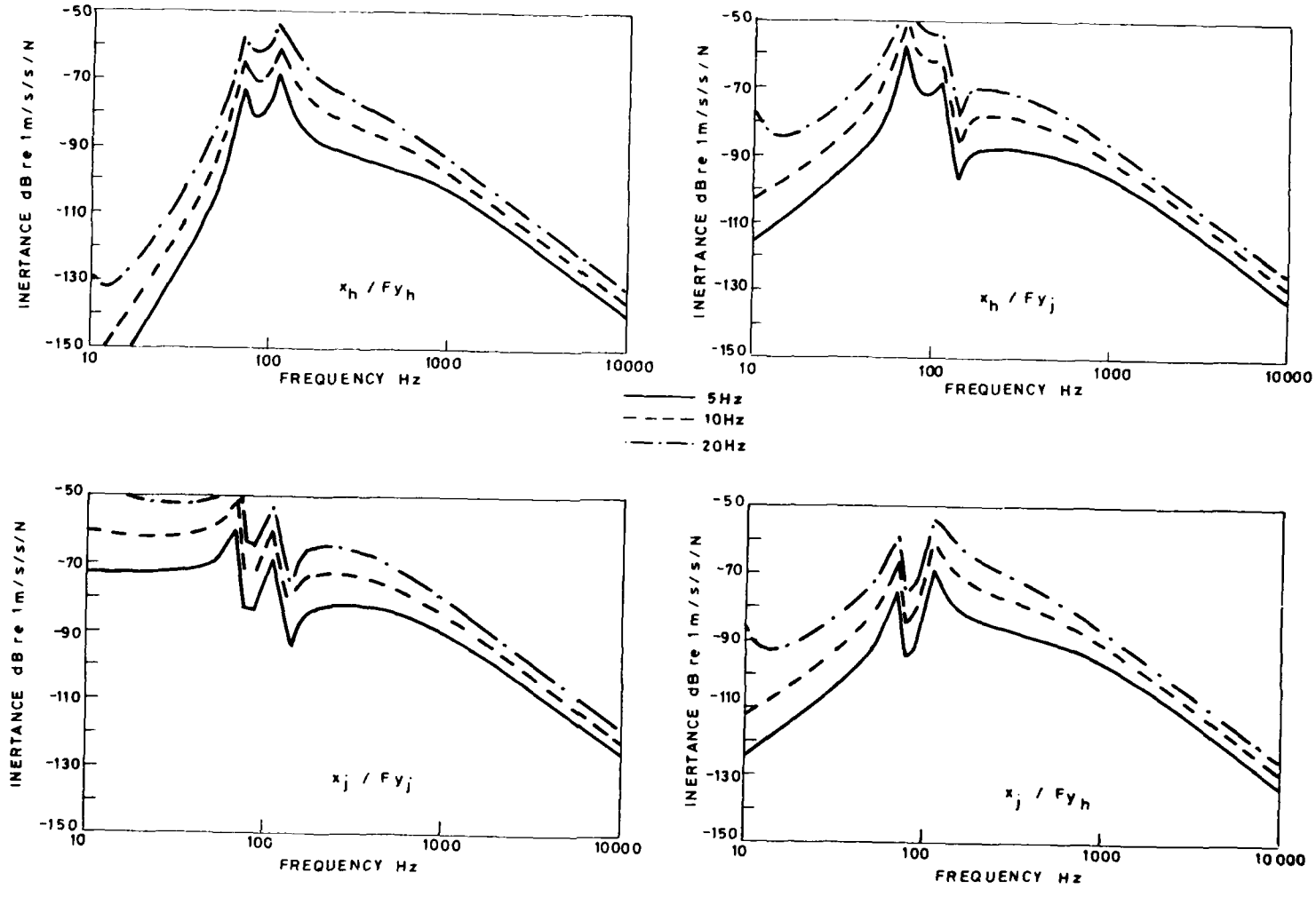

FIG. 19 PREDICTED CROSS INERTANCES FOR OM13 OIL AT VARIOUS SHAFT RATES (LOW LOAD) SHORT 360° BEARING

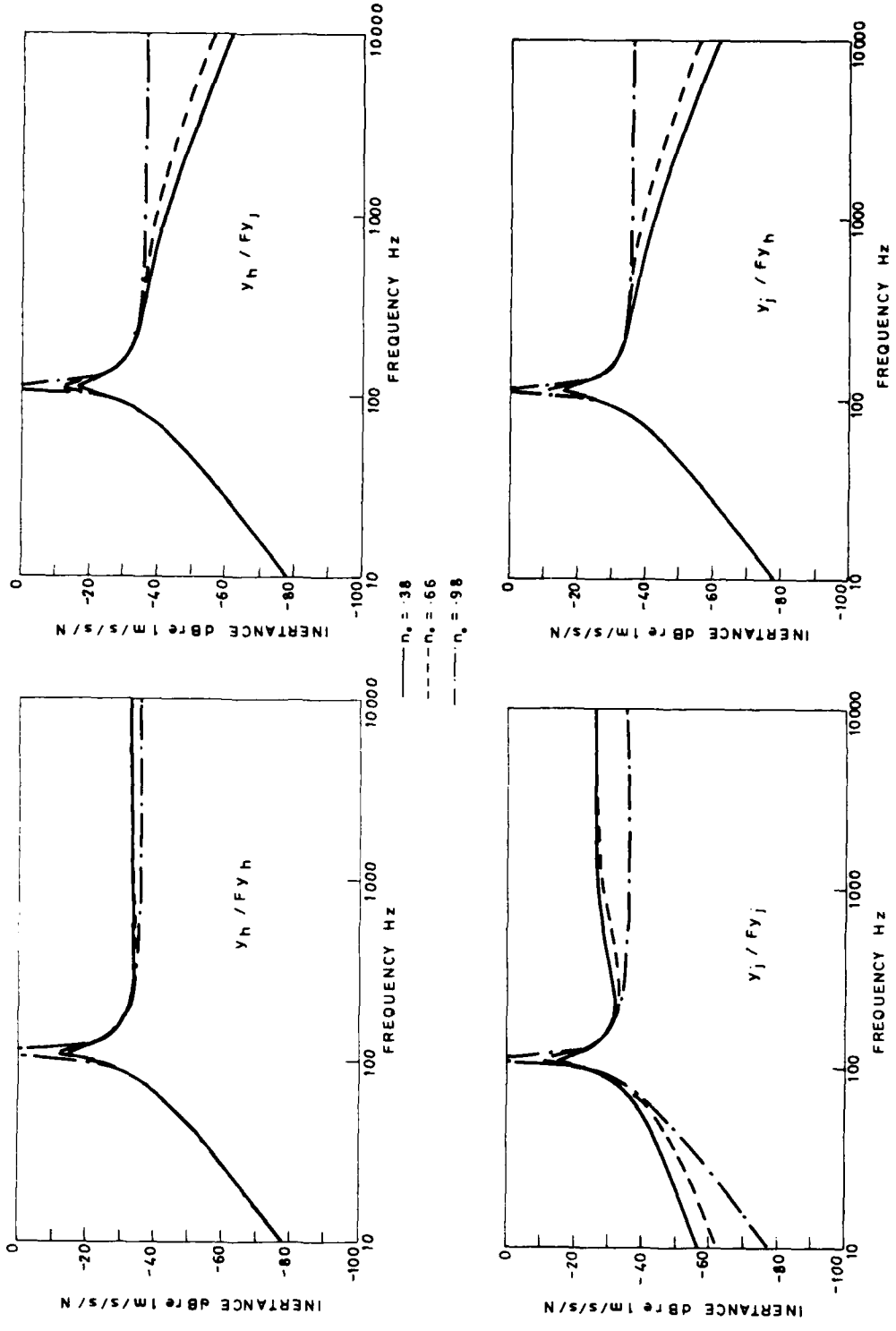

FIG. 20 VARIATION OF PREDICTED POINT AND TRANSFER INERTANCES WITH ECCENTRICITY

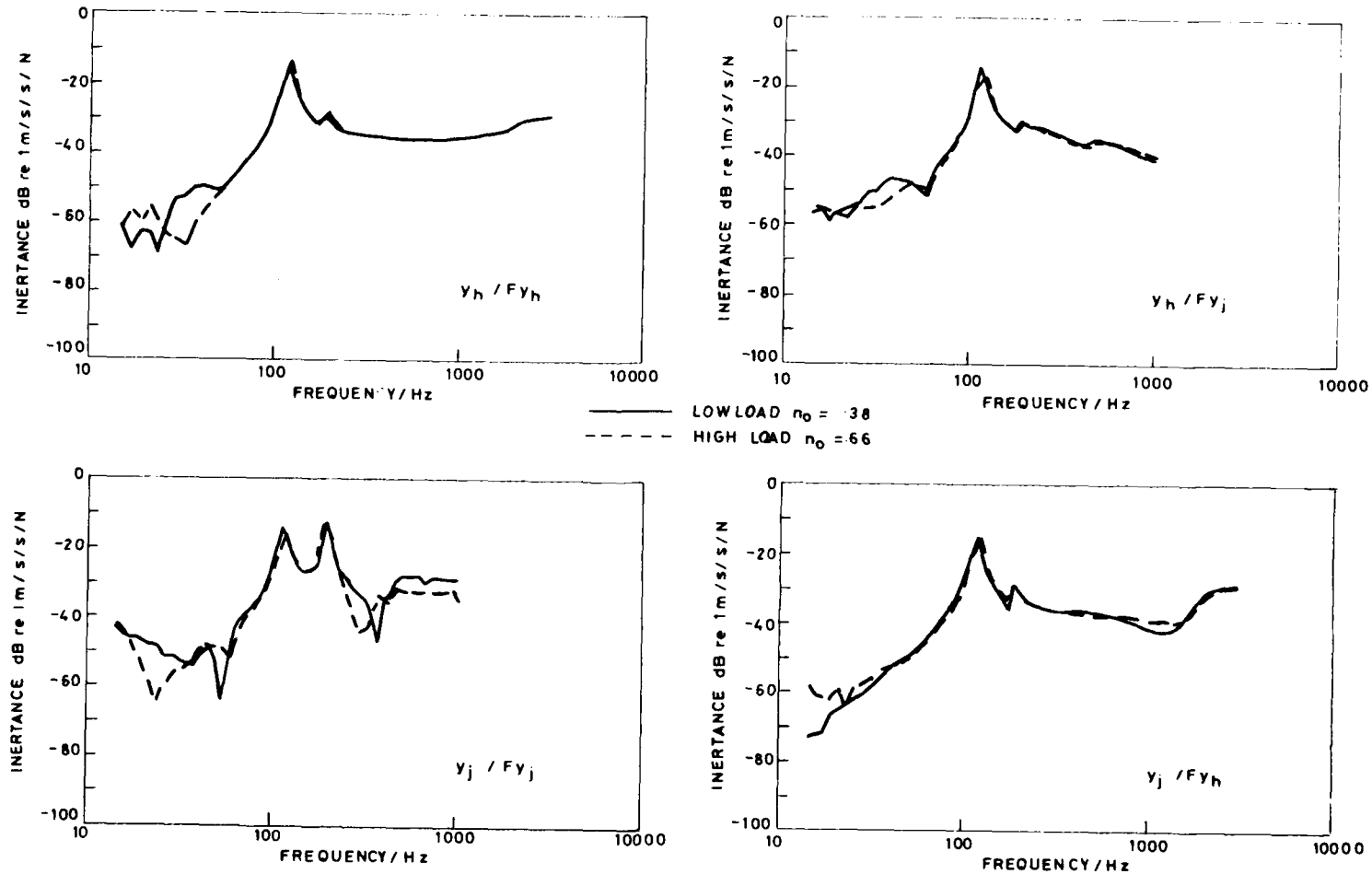

FIG 21 VARIATION OF MEASURED POINT AND TRANSFER INERTANCES WITH ECCENTRICITY
OM 13 OIL 5Hz SHAFT RATE

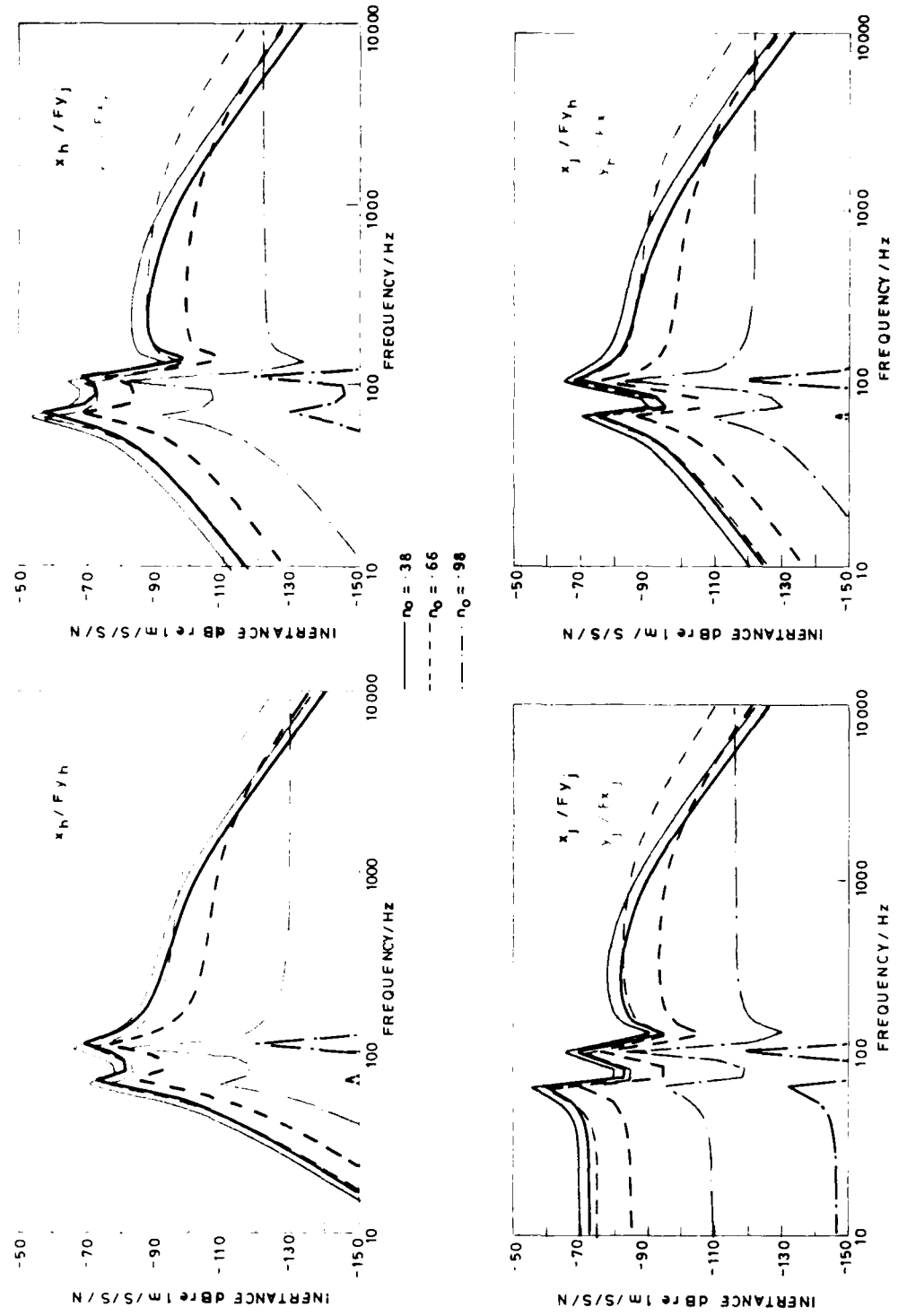

FIG. 22 VARIATION OF PREDICTED CROSS INERTANCES WITH ECCENTRICITY (PARAMETERS AS FOR OM13 OIL AT 5Hz SHAFT RATE)

10. MODULATION

Theory

Part 1 [3, see also 4] developed a theory to describe how the non-linear components of the bearing coefficients modulated the response to a force at frequency ω by producing sidebands at intervals of the out of balance force frequency taken as the shaft rate Ω. The theory was applied to a 360° "long" bearing in the region where the system is dominated by the stiffness of the housing and gave the levels of the upper sidebands (frequency $\omega+\Omega$) relative to the fundamental response level as

$$\frac{x_j(\omega+\Omega)}{x_j(\omega)} = \Delta$$

$$\frac{y_j(\omega+\Omega)}{y_j(\omega)} = \Delta \frac{k\Omega^2}{4K\omega^2}$$

$$\frac{x_h(\omega+\Omega)}{x_h(\omega)} = \Delta$$

$$\frac{y_h(\omega+\Omega)}{y_h(\omega)} = \Delta \frac{m_j\Omega^2}{4K}$$

where $$\Delta = \frac{3n_0F_0}{4Kc\omega}\frac{\Omega}{}$$

It was assumed that the dynamic force was acting on the journal (F_{yj}) and that the bearing stiffness was of the same order or greater than that of the housing ($K \geq k$). These expressions should therefore be valid in the case when OMD 113 oil was used. Unfortunately, as the rotor was inaccessible there was no way of measuring the out of balance force F_0. The theory does predict, however, that the levels of the upper sidebands should differ according to the relative directions of the applied force and measured response: Using the bearing parameters given in Table 3 it was estimated that for a forcing frequency of around 80Hz, say, the first sidebands on the response in the direction of the applied force would be some 20dB (on the journal) to 40dB (on the housing) lower than the responses perpendicular to the applied force.

Part 1 [3] also reports a numerical investigation of the modulation effects of a theoretical bearing for which the housing behaviour is determined by its stiffness. These calculations have been repeated using the parameters relevant to the bearing test rig assuming an out of balance force around 2% of the static load. The results suggest that for a dynamic force at around 80Hz the first order sidebands would be some 70dB to 80dB and some 50dB to 60dB down on the fundamental in directions parallel and perpendicular respectively to the applied force.

Experiment

An experiment was performed on the test rig to investigate these predictions. The rig was run at a shaft rate of around 10Hz and the accelerations were measured at all four response positions for the case of (i) no external force, (ii) with an 81Hz 20N force applied to the journal and (iii) with an 81 Hz 25N force applied to the housing. The results for (i) and (ii) are shown in Figure 23. Two sets of lines can be seen and are due to out of balance at shaft rate and at the belt drive frequency ($f_{belt} \simeq 2/3\ f_{shaft}$), the latter being the more pronounced. The forced response at 81Hz is only some 40db to 50dB above the general noise level in the direction of the applied force and less than this in the perpendicular direction and hence the sidebands due to modulation (if present) were not apparent. The differential between the forced response and background noise could not be significantly increased to render the sidebands visible. Attempts at increasing the applied force introduced distortion while increasing the number of averages used in producing the spectra had no significant effect.

An effect which was not expected is the upward shifting of the system frequencies by about 1 Hz when the external force is applied. (Although these appear to become sidebands to the fundamental in the example in Figure 21 this is not the case; a second set of measurements with the input force at 83Hz showed the same 1 Hz shift to the right but in this case it was clear that the lines were not becoming sidebands to the fundamental). This effect could not be explained and requires further investigation.

The frequency shifting effect was also observed when the force was applied to the journal. However, the results are not shown in figure 23 . In this case the measurements showed that when the rig was running the input force itself had sidebands on the fundamental at intervals of shaft rate and belt rate and these were most likely due to out of balance effects. As the input force was itself modulated it would be impossible to distinguish whether any apparent modulation on the response was genuinely due to bearing induced modulation or due to response to the modulated force.

A second set of measurements was performed forcing the system at 553Hz which occurs in the region where the massive housing approximation applies. The results are shown in Figure 24 . In this region the system noise is essentially featureless so that lines introduced in response to the applied force could clearly be identified. These lines were sidebands to the fundamental at frequency intervals of both shaft rate and belt drive frequency. Examination of the drive force spectrum showed that when forcing on the housing the input force consisted of a single line at the specified frequency and this was some 80dB above the flat background noise level. As there was no sign of modulation on the input force itself in this case the sidebands seen on the response could confidently be attributed to modulation induced by the bearing.

Appendix 4 develops the theory derived in Part 1 [3] to explore the effects of modulation at the frequencies for which the "massive housing" approximation applies. In this case it is shown that for a stiff bearing ($K=C\Omega/2 \gg \omega\Omega(m_j+m_h)/2$) which is forced on the housing at a frequency well above the out of balance frequency ($\omega>\Omega$) the amplitude of the upper sideband relative to that of the fundamental is given by

$$\frac{x_j(\omega+\Omega)}{x_j(\omega)} = \Delta^*$$

$$\frac{y_j(\omega+\Omega)}{y_j(\omega)} = \Delta^* \frac{Km_j m_h}{c^2(m_j+m_h)}$$

$$\frac{x_h(\omega+\Omega)}{x_h(\omega)} = \Delta^*$$

$$\frac{y_h(\omega+\Omega)}{y_h(\omega)} = \Delta^* \frac{Km_j^2}{c^2(m_j+m_h)}$$

where $$\Delta^* = \frac{3F_o n_o K^2 m_h}{2c\omega^2 c^3(m_j+m_h)}$$

Inserting the relevant parameters for the test rig running at 10Hz suggests that the relative levels of the sidebands in the direction of the applied force should be some 50dB lower than those perpendicular to the applied force. Examination of Figure 24 shows this is not observed in practise.

FIG 23 MODULATION INVESTIGATION FORCING HOUSING AT 81 Hz

FIG. 24 MODULATION INVESTIGATION FORCING HOUSING AT 553 Hz

11. DISCUSSION

Linear Transfer Functions

The agreemnt obtained between the predicted inertances and those measured when forcing on the housing is highly satisfactory (Figure 13a) and lends much credence to the theory developed. While the results obtained when forcing the journal (Figure 13b) are consistent with the theory it is unfortunate that they were very noisy at low frequencies and, the point inertance in particular, suffered from the axial effects at higher frequencies. These effects also prevented a conclusive check on the reciprocity of the bearing. Nevertheless, since the differences between the two transfer functions are small in regions not affected by spurious effects, it seems reasonable to conclude that reciprocity does apply.

Measurements on the cross inertances were disappointing since the noise on these precluded a validation of the theory. It is fair to comment, however, that the true cross transfer functions of the bearing will be very low, as predicted.

In retrospect, the problems arising from noise and axial effects may have been overcome to some extent by improvements to the test rig. Such improvements will be discussed later in this section.

Non Linear Effects - Modulation

The theory developed in Part 1 and extended here in Appendix 4 predicts that the out of balance effects within a bearing can modulate a transmitted force inducing sidebands at intervals of the out-of-balance frequency. Experimental work on the bearing test rig confirmed that the responses to a pure monotone force applied to the bearing could be modulated in this way. Unfortunately when applied to the journal the force itself was modulated so that the modulation seen on response could not be uniquely attributed to the bearing.

Quantitative agreement between the theory and experimental results was not achieved. As there was no provision for measuring the out-of-balance force on the test rig the levels of the sidebands relative to the fundamental could not be predicted. The only numerical test available was the comparison of the modulated responses in directions parallel and perpendicular to the applied force: The theory estimated that the relative levels of the sidebands in the directions of the applied force should be some 50dB lower than those perpendicular to the applied force when forcing at around 550Hz. Examination of the measured results shown in Figure 24 shows that the relative responses on the journal are the same for both directions while those on the housing differ by around 15dB.

Thus, while experiment does confirm that modulation can occur on transmission across the bearing, the results do not conform with the theoretical predictions. The theory derived was for a 360° 'Long' bearing. Better agreement might be obtained using the short bearing approximation. The short bearing coefficients were used when defining the linear transfer functions and have been seen to give excellent agreement with measured results. The corresponding coefficients for the long bearing were some three times larger and caused the onset of decoupling to be shifted to higher frequencies so that the agreement between experiment and theory was not so good numerically, although they were qualitatively consistent. These results

have not been presented as the short bearing approximation gave better agreement and, since the bearing had an L/D ratio of unity and the oil supply ensured an axial flow, was probably more valid. It therfore seems quite likely that the short bearing approximation would lead to better agreement in the modulation results; this should be explored further.

As the modulation theory has not been substantiated by the test rig results, it cannot be sensibly applied to the bearings in marine gearboxes. Thus although the sidebands observed in these gearboxes [3] may well be introduced by the bearings, this cannot yet be confirmed.

Improvements to the test rig

Several deficiencies have been identified in the bearing test rig which have limited the value of the measurements made. Some improvements could have been effected by slightly different design of the rig; these will be discussed briefly here as they may serve to guide future research.

A major difficulty in designing the test rig was the method for inputting a known force onto the journal. While the method used afforded some satisfaction the results were noisy and complicated by the axial resonance. The only axial constraint on the design rig was that due to the bearing seals and the mechanical restraint of the forcing arm.

The forcing system was very difficult to set up due to the limited space available inside the stator. The rig could have been built on a larger scale in order to make the interior more accessible. Some errors may have been introduced by misalignment of the internal transducers; these would have been overcome by improved accessibility.

Another major set back was noise, particularly on the cross inertances. To overcome this the input force would need to be increased, this could not be done with the equipment available without producing unwanted distortion to the input force.

Experiments on the test rig were halted when metallic deposits began to appear in the drained oil. On dismantling the test rig the outer surface of the test bearing was found to be badly pitted. A more substantial surface than the sprayed white metal used would have allowed further tests to be taken; The effects of modulation could then have been explored in more detail.

Another deficiency of the test rig was that there was no provision for measuring the out-of-balance forces. Although the rotor itself was not accessible, the drive plates connected to the ends of the journal could possibly have been modified to facilitate the use of test masses to give a measure of the shaft rate out of balance.

12. CONCLUSIONS

The theory developed in Part 1 to describe the linear transfer functions of a hydrodynamic bearing has been supported by measurements made on the experimental test rig.

It has been shown that an operational bearing may affect vibrations being transmitted across it: While bearings are often assumed to be rigid to vibration it is possible for the bearing to act as a damper if the stiffness and damping coefficients of the oil film are sufficiently low. This suggests a suitably designed bearing could be used to reduce the level of vibration being transmitted. However, as a reduction in the bearing stiffness would lower the static load capacity (See section 7) some compromise would have to be reached; Further discussion of the operational feasibility of a low stiffness bearing is beyond the scope of this work.

The theory also predicts that in general the transfer functions across the bearing should be reciprocal. The only exception to this is for high eccentricity bearings (n_0= 0.7, say) and even then only the cross inertances are affected.

A theory was developed in Part 1 to describe how non-linear effects in bearings can modulate transmitted vibrations by introducing sidebands to the fundamental at intervals of the out-of-balance frequency. Experimental results were not consistent with the theoretical predictions, but this is most likely due to the application of the 'long' bearing approximation to a test bearing which was, probably, 'short'. The measurements did, however, confirm that modulation can be introduced on transmission across bearings. Thus bearings could well be the source of the modulation observed in marine gearboxes.

L.V.EMBLING (HSO)
C.J.JENKINS (SSO)
P.J.MEYER (ASO)

ACKNOWLEDGEMENT

The authors wish to thank J.R. Soper for his invaluable assistance and advice in the experimental aspects of this study, and D. Cordner for performing the numerical calculations of modulation levels.

REFERENCES

1. WHITE, M.F. Vibration transmission characteristics of bearings related to machinery condition monitoring. ISVR Technical Report No 96 Dec 1977.

2. KINNS, R. The deduction of bearing forces in rotating machinery. Proc. Euromech Colloquium 122 Paris (1979).

3. JENKINS, C.J., EMBLING, L.V. and CORDNER, D.A. The generation and transmission of vibration in plain cylindrical bearings. (U) Part 1. Theory. Unpublished MOD (PE) report.

4. JENKINS C.J., EMBLING L.V. and CORDNER D.A. The prediction and measurement of bearing transfer functions at high frequencies.
Third International Conference on Vibrations in Rotating Machinery. York, 1984:
I. Mech. E. Conference publications 1984-10 paper C268/84.

5. HERSEY, M.D. Theory and research in lubrication - Foundations for future developments. John Wiley & Sons Inc. (1966)

6. JENNINGS, U.D. and OCVIRK, F.W. The simulation of bearing whirl on an electronic-analogue computer. Trans ASME. J. Basic Engineering, 84, 503-510 (1962).

7. HOLMES, R. Oil whirl characteristics of a rigid rotor in 360° journal bearings. Proc. Inst. Mech. Eng. 177, 291, (1963)

8. BANNISTER, R.H. A theoretical and experimental investigation illustrating the influence of non-linearity and misalignment on the eight oil film force coefficients. Inst. Mech. Eng. Conference Vibrations in Rotating Machinery C219/76, Cambridge (1976)

9. PARKINS, D.W. Theoretical and experimental determination of the dynamic characteristics of a hydrodynamic journal bearing. Trans ASME. J. Lub. Tech. 101, 129, (1979).

10. FLACK, R.D. and ROOKE,J.H. A theoretical - experimental comparison of the synchronous response of a bowed rotor in five different sets of fluid film bearings. J.Sound & Vibn. 73(4), 505, (1980).

11. COOKSON, R.A. and KOSSA, S.S. The vibration isolating properties of uncentralised squeeze-film damper bearings supporting a flexible rotor. Trans ASME. J. Eng. for Power, 103, 781, (1981).

12. DEFENCE STANDARD. Fuels, lubricants and associated products. DEF STAN 01-5/4-HMSO. (August 1981).

13. CAMERON, A. Basic lubrication theory, 3rd Edition, Ellis Horwood Series in Engineering Science, John Wiley and Sons, (1981).

APPENDIX 1. VIBRATIONS IN BEARINGS.

The major causes of vibration in bearings are journal out of balance and fluid film whirl.

Vibration due to out of balance is sometimes known as synchronous whirl. In this case the journal rotates about its geometric centre until reaching an "inversion" speed at which it begins to rotate about an axis through the centre of gravity (Figure A1) thus causing vibration at shaft rate.

For a properly balanced rotor the main cause of vibration is fluid film whirl which is purely hydrodynamic in origin if the rotor is rigid. If static equilibrium were maintained between the hydrodynamic forces of the fluid and the load on the journal then the centre of the journal would remain fixed relative to the bearing. The locus of possible positions of the journal centre is approximately a semi-circle in the bearing clearance [6] - Figure A2a. Under certain conditions static equilibrium is no longer maintained and the journal centre may trace a steady state closed path as indicated in Figure A2b; this is the condition known as stable whirl and is similar in effect to out of balance. In some cases the dynamic state may be unstable and the journal centre traces an outwardly spiralling whirl path (Figure A2c); since in most practical bearings the orbital frequency of the whirl path is approximately half the shaft rate this is often known as half frequency whirl. If the journal axis remains parallel with the bearing the whirl is said to be translatory; if the journal axis gyrates the whirl is conical.

As the shaft rate is increased it passes through a critical speed corresponding to the resonance frequency of the system, often approximated by $(1/2\pi)\sqrt{(\text{journal stiffness/journal mass})}$. At speeds above twice the critical speed resonant whirl, or whip, may occur. This is a complicated effect arising from both the flexibility of the shaft and the oil film hydrodynamics. In this case the whirl frequency approximates to the critical frequency.

The frequencies of the different types of oil whirl are summarised in Figure A3.

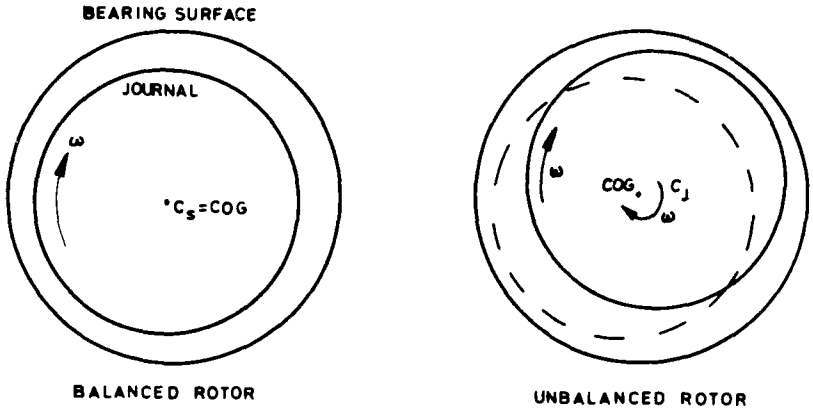

FIG. A1 VIBRATION DUE TO JOURNAL OUT OF BALANCE

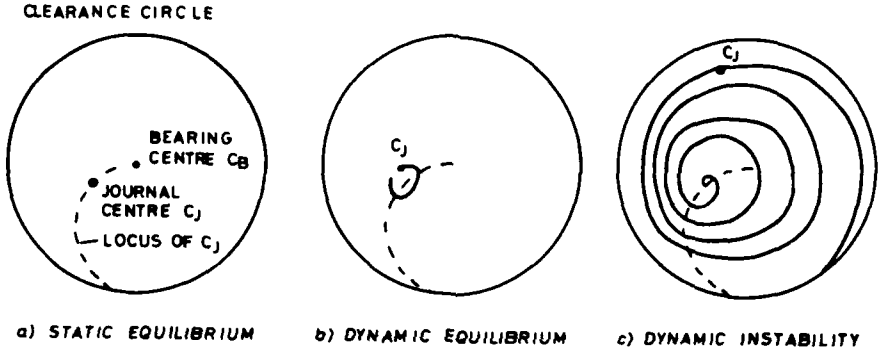

FIG. A2 LOCII OF JOURNAL CENTRES UNDER FLUID FILM WHIRL

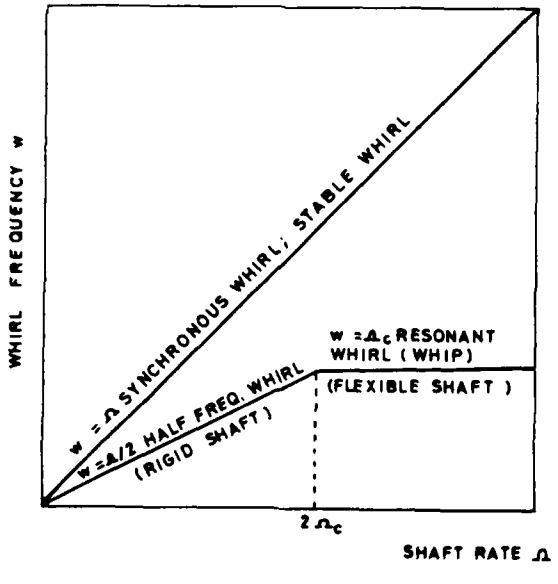

FIG. A3 WHIRL FREQUENCIES IN RELATION TO SHAFT RATE

APPENDIX 2. OIL FLOW THROUGH BEARINGS.

The oil flow in hydrodynamic bearings consists of two components, the flow due to the pumping action of the bearing and the axial flow due to leakage:

Pumped Flow

The oil flow rate due to the pumping action of a 360° bearing is given approximately (Chapter 7 of [13]) by

$$Q_p = \frac{UcLn}{2} \qquad \text{A2.1}$$

where $U = R\Omega$ is the tangential velocity of the journal surface.

Leakage Flow

This is the oil flow resulting from the pressure oil feed and depends on the external feed pressure and the geometry of the feed port as well as the oil viscosity and bearing clearance in the vicinity of the feed port. Oil is normally fed into the bearing in one of three ways which are i) a circumferential groove, ii) a feed hole and iii) feed pockets. Different expressions apply for each of these cases (Chapter 7 of [13]) for the leakage oil flow out of both ends of the bearing; these are summarised in Table A2.

TABLE A2. OIL FLOW RATES FOR VARIOUS INLET PORTS.

Circumferential groove	$\frac{2\pi c^3 p_0 R}{3 \mu L}\left[1 + \frac{3n^2}{2}\right]$	
Entry port	$\frac{Rc^3 p_0 Q^*}{12 \mu L}$	Q^* is a coefficient determined by port geometry.
Hole, diameter D at azimuth angle θ	$\frac{h^3 p_0 D Q_d^*}{12 \mu L}$	$Q_d^* \simeq 1.2 + 11 \frac{D}{L}$ $h = c(1 + n \cos\theta)$
Axial slot, length l infinitely narrow.	$\frac{h^3 p_0 R Q_{go}^*}{6 \mu L}$	$Q_{go}^* \simeq 4\left[\frac{L}{l} - 1\right]^{-\frac{1}{3}}$
Two slots	$\frac{c^3 p_0 R \zeta Q_{go}^*}{6 \mu L}$	$\zeta = 2(1+3n^2-3n^4)$
Two grooves finite width b length l	$\frac{c^3 p_0 R \zeta}{6 \mu L}\left[Q_{go}^* + \frac{2b}{R(1-l/L)}\right]$	

Measurement of clearance

Cameron [13] recommends that the oil flow rate from the bearing be used to give an estimation of the bearing clearance which often closes in as the bearing temperature increases. It is suggested that after running at the required temperature the journal should be rapidly brought to rest and the static oil flow out of the bearing be measured immediately. This procedure eliminates the pumping component so that the clearance may be evaluated directly from the appropriate expression in Table A2.

With the journal at rest the eccentricity ratio becomes equal to unity so that h=2c for a hole at the top of the bearing and hence

$$Q = \frac{8c^3 p_0 D \, Q_d^*}{12 \mu L}$$

APPENDIX 3. BEARING TRANSFER FUNCTIONS.

Part 1 of this report [3, see also 4] showed that the bearing response {x} to a harmonic force {F} is given by

$$\{x\} = [H]^{-1} \{F\} \qquad \text{A3.1}$$

where

$$[H] = -\omega^2 \begin{bmatrix} [m_j] & 0 \\ 0 & [m_h] \end{bmatrix} + \begin{bmatrix} [k_j] & 0 \\ 0 & [k_h] \end{bmatrix} + \begin{bmatrix} -[K] & -[K] \\ [K] & [K] \end{bmatrix} + j\omega \begin{bmatrix} -[C] & [C] \\ [C] & -[C] \end{bmatrix} \qquad \text{A3.2}$$

and $[m_j]$ and $[m_h]$ are the journal and housing mass matrices and
$[k_j]$ and $[k_h]$ are the journal and housing stiffness matrices.
[K] and [C] are the journal stiffness and damping matrices which, for bearings of low eccentricity, are given by

$$[K] = \begin{bmatrix} 0 & \frac{A\Omega}{2c} \\ -\frac{A\Omega}{2c} & 0 \end{bmatrix} \quad \text{and} \quad [C] = \begin{bmatrix} \frac{-A}{c} & \\ & \frac{-A}{c} \end{bmatrix} \qquad \text{long 360° bearing}$$

$$[K] = \begin{bmatrix} 0 & \frac{B\pi\Omega}{2c} \\ -\frac{B\pi\Omega}{2c} & 0 \end{bmatrix} \quad \text{and} \quad [C] = \begin{bmatrix} \frac{-B\pi}{c} & 0 \\ 0 & \frac{-B\pi}{c} \end{bmatrix} \qquad \text{short 360° bearing} \qquad \text{A3.3}$$

where $$B = \frac{RL^3\mu}{c^2} = \frac{A}{12\pi}\left[\frac{L}{R}\right]^2$$

so that for a bearing with L/(2R) ratio of unity the short and long stiffness and damping coefficients differ only by a factor of three.

Under the action of a single unidirectional force $\{F\}^T = \{0....F_j...0\}$ the transfer functions are given by

$$\frac{x_i}{F_j} = \frac{\alpha_{ij}}{|H|} \qquad \text{A3.4}$$

where α_{ij} are the cofactors of the element H_{ji}.

To simplify the calculation of the cofactors α_{ij} and the determinant of the matrix [H] two limiting cases were considered where the rotor was assumed to be rigid and the housing was taken as being either very stiff or very massive.

i) Massive journal in very stiff housing

The effects of journal stiffness and housing mass were neglected so that

$$\alpha_{11} = \alpha_{22} = \left(k - m_j\omega^2 \right)\left[\left[\frac{A\Omega}{2c}\right]^2 - \left[\frac{A\omega}{c}\right]^2 \right] - k^2 m_j \omega^2 - i\,\frac{A\omega k}{c}\left(2m_j\omega^2 - k\right)$$

TABLE A3.1. LINEARISED BEARING COEFFICIENTS.

	Long 360°	Short 360°	Short 180°
K_{xx}	0	0	$\frac{-\chi n_0(2+n_0^2(D-1))}{(1-n_0^2)^3}$
K_{xy}	$\frac{A\Omega}{c(2+n_0^2)(1-n_0^2)^{1/2}}$	$\frac{\pi B\Omega}{2c(1-n_0^2)^{3/2}}$	$\frac{-\chi\pi(-1+2n_0^2+n_0^4(D-1))}{(1-n_0^2)^{7/2}}$
K_{yy}	0	0	$\frac{-\chi n_0(1+n_0^2(1+2D)+n_0^4(2D-2))}{(1-n_0^2)^4}$
K_{yx}	$\frac{-A\Omega(2-n_0^2+2n_0^4)}{c(2+n_0^2)^2(1-n_0^2)^{3/2}}$	$\frac{-\pi B\Omega(1+2n_0^2)}{2c(1-n_0^2)^{5/2}}$	$\frac{-\chi\pi(1+n_0^2(1+2D)+n_0^4(2D-2))}{4(1-n_0^2)^{7/2}}$
C_{xx}	$\frac{-A}{c(1-n_0^2)^{3/2}}$	$\frac{-\pi B(1+2n_0^2)}{c(1-n_0^2)^{5/2}}$	$\frac{-\chi\pi(1+n_0^2(2-D))}{2\Omega(1-n_0^2)^{5/2}}$
C_{xy}	0	0	$\frac{-\chi 2n(1+n_0^2(2-D))}{\Omega(1-n_0^2)^3}$
C_{yy}	$\frac{-2A}{c(2+n_0^2)(1-n_0^2)^{1/2}}$	$\frac{-\pi B}{c(1-n_0^2)^{3/2}}$	$\frac{-\chi\pi(1+n_0^2(3D-2)+n_0^4)}{2\Omega(1-n_0^2)^{7/2}}$
C_{yx}	0	0	$\frac{-\chi 2n_0(1+n_0^2(2-D))}{\Omega(1-n_0^2)^3}$

$A = \frac{12\mu R^3 L\pi}{c^2}$ $\quad B = \frac{RL^3\mu}{c^2}$ $\quad \chi = \frac{\Omega B}{c}\sin^2\Phi$ $\quad D = \frac{16}{\pi^2}$

TABLE A3.2. NoON LINEAR TERMS IN BEARING COEFFICIENTS

	Long 360°	Short 360°
K_{xx}	0	0
K_{xy}	$\frac{3\varepsilon n_0^3 A\Omega}{c^2(2+n_0^2)^2(1-n_0^2)^{3/2}}$	$\frac{3B\pi\varepsilon n_0\Omega}{2c^2(1-n_0^2)^{5/2}}$
K_{yx}	$\frac{-3A\varepsilon n_0^3(8-2n_0^2+3n_0^4)}{2c^2(2+n_0^2)^3(1-n_0^2)^{5/2}}$	$\frac{-B\pi\varepsilon n_0(9+6n_0^2)}{2(1-n_0^2)^{7/2}}$
K_{yy}	$\frac{-3A\Omega\gamma n_0^2}{2c^2(2+n_0^2)^2(1-n_0^2)^{3/2}}$	0
C_{xx}	$\frac{-3A\varepsilon n_0}{c^2(1-n_0^2)^{5/2}}$	$\frac{-B\pi\varepsilon n_0(9+6n_0^2)}{c^2(1-n_0^2)^{7/2}}$
C_{xy} C_{yx}	$\frac{-3A\gamma n_0}{c^2(2+n_0^2)(1-n_0^2)^{3/2}}$	$\frac{-3\pi B\gamma n_0}{c^2(1-n_0^2)^{5/2}}$
C_{yy}	$\frac{-6An_0^3\varepsilon}{c^2(2+n_0^2)^2(1-n_0^2)^{3/2}}$	$\frac{-3\pi B\varepsilon n_0}{c^2(1-n_0^2)^{5/2}}$

$$\alpha_{12} = -\alpha_{21} = k^2 K$$

$$\alpha_{13} = \alpha_{24} = \alpha_{31} = \alpha_{42} = (k - m_j\omega^2)\left[K^2 - (C\omega)^2\right] - i\,C\omega\; km_j\omega^2$$

$$\alpha_{14} = -\alpha_{23} = \alpha_{32} = -\alpha_{41} = km_j\omega^2 K$$

$$\alpha_{34} = -\alpha_{43} = (m_j\omega^2)^2 K$$

$$\alpha_{33} = \alpha_{44} = (k - m_j\omega^2)\left[K^2 - (C\omega)^2\right] + k(m_j\omega^2)^2 + i\,C\omega\, m_j\omega^2(m_j\omega^2 - 2k) \qquad \text{A3.5}$$

and

$$|H| = (k - m_j\omega^2)^2\left[K^2 - (C\omega)^2\right] + k^2(m_j\omega^2)^2 - i\,C\omega\, 2km_j\omega^2(k - m_j\omega^2) \qquad \text{A3.6}$$

where the housing stiffness k was assumed to be the same in the x and y directions ($k_x = k_y$) and $K = A\Omega/2c$ $C = A/c$ (long 360° bearing).

By setting $|H| = 0$ resonances were predicted at frequencies $\omega = \Omega/2$ (whirl) and $\omega = \sqrt{(k/m_j)}$.

The frequency range for which the stiff housing approximation applies on a real system is limited by the system resonance. Thus, since we are interested only in frequencies above shaft rate

$$\Omega < \omega < \underbrace{\left[\frac{k}{(m_j + m_h)}\right]^{1/2}}_{\text{true system resonance}} < \underbrace{\left[\frac{k}{m_j}\right]^{1/2}}_{\text{predicted resonance for stiff housing.}} \qquad \text{A3.7}$$

In this region the transfer functions for a dynamic force applied to the journal in a vertical direction become

$$\frac{x_j}{F_{yj}} = \frac{-K}{C^2\omega^2} \qquad \frac{x_h}{F_{yj}} = \frac{-2m_jK}{kC^2} \qquad \text{A3.8}$$

$$\frac{y}{F_{yj}} = \frac{1}{k} + \frac{m_j}{C^2} + \frac{i}{\omega C}$$

$$= \frac{1}{k} + \frac{m_j\Omega^2}{4K^2} + \frac{i\Omega}{2\omega K} \simeq \frac{1}{k} \qquad K^2 \gg m_j\Omega^2 k\;;\quad K \gg \frac{\Omega}{\omega}k$$

$$\simeq \frac{i\Omega}{4\omega K} \qquad K^2 \gg m_j\Omega^2 k\;;\quad K \ll \frac{\Omega}{\omega}k$$

$$\simeq \frac{m_j\Omega^2}{4K^2} \qquad K^2 \ll m_j\Omega^2 k\;;\quad K \gg m_j\Omega\omega$$

A3.9

$$\frac{y_h}{F_{yh}} = \frac{1}{k} + \frac{(m_j\omega^2)^2}{k(\omega C)^2} + \frac{i2m_j\omega^2}{k\omega C} \qquad \text{A3.10}$$

$$\frac{y_h}{F_{yh}} = \frac{1}{k} + \frac{i\, m_j\omega^2}{C\omega k}$$

$$\simeq \frac{1}{k} \qquad \omega C >> m_j\omega^2$$

$$\simeq \frac{im_j\omega^2}{C\omega k} \qquad \omega C << m_j\omega^2 \qquad \text{A3.11}$$

Note the bearing is rigid at lower frequencies but loses this rigidity when the stiffness decreases.

ii) Massive journal in massive housing.

The effects of both journal and housing stiffness were neglected giving

$$\alpha_{11} = \alpha_{22} = -(m_j + m_h)\omega^2\left[K^2 - (C\omega)^2\right] - m_j m_h^2\omega^6 + i\,C\omega\, m_h\omega^4(2m_j + m_h)$$

$$\alpha_{33} = \alpha_{44} = -(m_j + m_h)\omega^2\left[K^2 - (C\omega)^2\right] - m_j^2 m_h\omega^6 + i\,C\omega m_j\omega^4(m_j + 2m_h)$$

$$\alpha_{12} = -\alpha_{21} = m_h^2\,\omega^4\,K$$

$$\alpha_{34} = -\alpha_{43} = m_j^2\,\omega^4\,K$$

$$\alpha_{13} = \alpha_{24} = \alpha_{31} = \alpha_{42} = -(m_j + m_h)\omega^2\left[K^2 - (C\omega)^2\right] + i\,C\omega\, m_j m_h\omega^4$$

$$\alpha_{14} = -\alpha_{23} = \alpha_{32} = -\alpha_{41} = -m_j m_h\omega^4\,K \qquad \text{A3.12}$$

$$|H| = \omega^4(m_j + m_h)^2\left[K^2 - (C\omega)^2 + \frac{\omega^4 m_j^2 m_h^2}{(m_j + m_h)^2} - i\,C\omega\,\frac{2m_j m_h\omega^2}{(m_j + m_h)}\right] \qquad \text{A3.13}$$

In this case only the whirl ($\omega = \Omega/2$) resonance is predicted.

These expressions simplify when the following conditions are satisfied

$$\Omega < \omega \quad ; \quad \omega < C\left[\frac{1}{m_j} + \frac{1}{m_h}\right] \qquad \text{A3.14}$$

The transfer functions are now given by

$$\frac{x_j}{F} = \frac{-m_h^2 K}{(m_j+m_h)^2(C\omega)^2} \qquad \frac{x_h}{F} = \frac{-m_j m_h K}{(m_j+m_h)^2(C\omega)^2} \qquad \text{A3.15}$$

$$\frac{y_j}{F} = \frac{-1}{\omega^2(m_j+m_h)} + \frac{m_j m_h^2}{(m_j+m_h)^2 C^2} - i\frac{m_h(2m_j+m_h)}{(m_j+m_h)^2\omega C}$$

$$= \frac{-1}{\omega^2(m_j+m_h)} \qquad \omega << \frac{C}{m_h}\left[1+\frac{m_h}{m_j}\right]^{1/2} ; \ \omega << \frac{C}{m_h}\frac{(m_j+m_h)}{(2m_j+m_h)}$$

$$= \frac{m_j m_h^2}{(m_j+m_h)^2 C^2} \qquad \omega >> \frac{C}{m_h}\left[1+\frac{m_h}{m_j}\right]^{1/2} ; \ \omega >> \frac{C(2m_j+m_h)}{m_j m_h}$$

$$= i\frac{m_h(2m_j+m_h)}{C(m_j+m_h)^2\omega} \qquad \frac{C(m_j+m_h)}{m_h(2m_j+m_h)} << \omega << \frac{C(m_j+m_h)}{m_j m_h} \qquad \text{A3.16}$$

$$\frac{y_h}{F} = \frac{-1}{\omega^2(m_j+m_h)} - i\frac{m_h m_j}{C(m_j+m_h)^2\omega}$$

$$= -\frac{-1}{\omega(m_j^2+m_h)} \qquad \omega << \frac{C(m_j+m_h)}{m_h m_j}$$

$$= \frac{-i\, m_h(m_j+2m_h)}{C(m_j+m_h)^2\omega} \qquad \omega >> \frac{C(m_j+m_h)}{m_h m_j} \qquad \text{A3.17}$$

At very high frequencies ($\omega >> 2C(m_j+m_h)/m_j m_h$) the transfer functions become

$$\frac{x_j}{F_{yj}} = \frac{K}{2m_j^2\omega^4} \ ; \quad \frac{x_h}{F_{yj}} = \frac{-K}{2m_j m_h \omega^4} \qquad \text{A3.18}$$

$$\frac{y_j}{F_{yj}} = \frac{-1}{m_j\omega^2} \ ; \quad \frac{y_h}{F_{yj}} = \frac{C}{m_j m_h \omega^3} \qquad \text{A3.19}$$

Note on reciprocity

Noting the symmetry of the inverse matrix [H] in the two sets of approximations discussed above it can be seen that for low eccentricity bearings

Point Receptance

$$\frac{x_j}{F_{xj}} = \frac{y_j}{F_{yj}} = \frac{\alpha_{11}}{|H|} \quad ; \quad \frac{x_h}{F_{xh}} = \frac{y_h}{F_{yh}} = \frac{\alpha_{33}}{|H|} \qquad \text{A3.20}$$

Transfer Functions

$$\frac{x_j}{F_{xh}} = \frac{y_j}{F_{yh}} = \frac{x_h}{F_{xj}} = \frac{y_h}{F_{yj}} = \frac{\alpha_{13}}{|H|} \qquad \text{A3.21}$$

Cross Transfer Functions

$$\frac{x_j}{F_{yh}} = \frac{-y_j}{F_{xh}} = \frac{x_h}{F_{yj}} = \frac{-y_h}{F_{xj}} = \frac{-\alpha_{41}}{|H|}$$

$$\frac{x_j}{F_{yj}} = \frac{-y_j}{F_{xj}} = \frac{-\alpha_{21}}{|H|} \quad ; \quad \frac{x_h}{F_{yh}} = \frac{-y_h}{F_{xh}} = \frac{-\alpha_{43}}{|H|} \qquad \text{A3.22}$$

where the forces are acting in isolation on the journal or housing in the x or y direction as indicated by the subscripts.

If the eccentricity is increased so that the bearing stiffness and damping matrices lose their symmetry then reciprocity will then cease to apply to the cross transfer functions.

APPENDIX 4. MODULATION THEORY FOR SYSTEM WITH MASSIVE HOUSING.

Part 1 of this report [3, see also 4] derived the levels of the sidebands due to modulation in response to a force applied to the journal at a frequency for which the housing inertance followed a stiffness line. This appendix extends that theory to consider the effect of a force applied to the housing and to explore modulation in the frequency range where the housing inertance follows the mass line.

FORCE APPLIED TO THE HOUSING.

For a force F of frequency ω applied to the housing in the direction of the static load and an out of balance force F_0 at frequency Ω equation V.21(a) of [4] becomes

$$F_1 = F_0 \sin \Omega t$$
$$F_2 = F_0 \cos \Omega t$$
$$F_3 = 0$$
$$F_4 = F \cos \omega t$$

Now from V.10 of [4] we have

$$G_i = \Delta_{ik} F_k = \frac{1}{c\nu^2} \left[M \right]^{-1}_{ik} F_k \qquad \text{A4.1}$$

and including the housing mass in [M] this gives

$$G_i = \frac{1}{c\nu^2} \frac{1}{m_j} F_i \qquad i=1,2$$

$$G_i = \frac{1}{c\nu^2} \frac{1}{m_h} F_i \qquad i=3,4 \qquad \text{A4.2}$$

so that

$$G_1 = \frac{1}{c\nu^2} \frac{1}{m_j} F_o \sin\Omega t \qquad G_2 = \frac{1}{c\nu^2} \frac{1}{m_j} F_o \cos\Omega t$$

$$G_3 = 0 \qquad G_4 = \frac{1}{c\nu^2} \frac{1}{m_h} F \cos\omega t \qquad \text{A4.3}$$

The linearised response (V.22) is now given by

$$u_i = (-1)^{1+i} \frac{r_{1i}(\Omega) F_o \sin\Omega t}{|R(\Omega)| m_j c\nu^2} + (-1)^{2+i} \frac{r_{2i}(\Omega) F_o \cos\Omega t}{|R(\Omega)| m_j c\nu^2} + (-1)^{4+i} \frac{r_{4i}(\omega) F \cos\omega t}{|R(\omega)| m_h c\nu^2} \qquad \text{A4.4}$$

while the perturbed response is still

$$v_i = \sum_{\substack{\text{resultant}\\ \text{frequencies}\\ \omega'}} \frac{(-1)^{1+i}}{|R(\omega)|} \left\{ r_{1i}(\omega') p_1 - r_{2i}(\omega') p_2 + r_{3i}(\omega') p_3 - r_{4i}(\omega') p_4 \right\}$$

with $$p_i = A_{ilk} u_k \dot{u}_l = \frac{1}{\nu} \left[M \right]^{-1}_{ij} \psi(x)_{jl} \dot{u}_l$$

However, retaining the housing mass in the matrix [M] we have

$$\left[M \right]^{-1}_{ij} = \delta_{ij} \frac{1}{M_i}$$

where

$$\delta_{ij} = 0 \quad i \neq j \qquad M_i = m_j \quad i=1,2$$
$$= 1 \quad i = j \qquad = m_h \quad i=3,4$$

A4.5

and so

$$p_1 = \frac{-m_h}{m_j} p_3 = \frac{3An_o}{m_j c\nu} \left[(u_1-u_3)(\dot{u}_1-\dot{u}_3) + \frac{1}{2} (u_2-u_4)(\dot{u}_2-\dot{u}_4) \right]$$

A4.6

$$p_2 = \frac{-m_h}{m_j} p_4 = \frac{3An_o}{m_j c\nu} (u_2-u_4)(\dot{u}_1-\dot{u}_3)$$

Thus the equation for the perturbed response (V.22a) becomes

$$v = \sum_{\substack{\text{resultant}\\ \text{frequencies}\\ \omega'}} \frac{(-1)^{i+1}}{|R(\omega')|} \left[\left\{ r_{1i}(\omega') - \frac{m_j r_{3i}(\omega')}{m_h} \right\} p_1 - \left\{ r_{2i}(\omega') - \frac{m_j r_{4i}(\omega')}{m_h} \right\} p_2 \right]$$

A4.7

MASSIVE HOUSING APPROXIMATION

The coefficients r_{ij} are the minors of the matrix [R]. Now since

$$\left[R \right] = \frac{1}{\nu^2} \left[M \right]^{-1} \left[H \right] \qquad \text{we find} \qquad R_{ij} = \frac{1}{\nu^2} \frac{1}{M_i} H_{ij}$$

and hence it can be shown that the minors r_{ij} of [R] are related to the minors α_{ij} of [H] by

$$r_{ij} = \frac{1}{\nu^6}\,\frac{1}{m_j m_h^2}\,\alpha_{ij} \qquad i=1,2$$

$$= \frac{1}{\nu^6}\,\frac{1}{m_j^2 m_h}\,\alpha_{ij} \qquad i=3,4 \qquad \text{A4.8}$$

while

$$|R| = \frac{1}{\nu^8}\,\frac{1}{m_j^2 m_h^2}\,|H|$$

Now the approximations for α_{ij} and $|H|$ are given in Appendix 3. These simplify when the bearing stiffness and damping are high

$$[K^2 - (C\omega)^2] \gg \frac{\omega^4 m_j^2 m_h^2}{(m_j + m_h)^2} \qquad \text{and} \qquad \gg \frac{C\omega\, 2m_j m_h \omega^2}{(m_j + m_h)}$$

So that for $\omega \gg \Omega$ and for $\omega = \Omega$ we now have

$$|H(\omega)| = -\omega^6 C^2 (m_j+m_h)^2 \qquad \text{and} \qquad H(\Omega) = \frac{-3}{4}\,\Omega^6 C^2 (m_j+m_h)^2$$

$$\alpha_{11}(\omega) = \alpha_{22}(\omega) = \alpha_{33}(\omega) = \alpha_{44}(w) = \omega^4 C^2 (m_j+m_h) \quad \text{or} \quad \frac{3}{4}\,\Omega^4 C^2 (m_j+m_h) \quad \text{when } \omega=\Omega$$

$$\alpha_{12} = -\alpha_{21} = \left(\frac{m_h}{m_j}\right)^2 \alpha_{34} = -\left(\frac{m_h}{m_j}\right)^2 \alpha_{43} = \omega^4 m_h^2 K \quad \text{or} \quad \Omega^4 m_h^2 K \quad \text{when } \omega=\Omega$$

$$\alpha_{13} = \alpha_{24} = \alpha_{31} = \alpha_{42} = \omega^4 C^2 (m_j+m_h) \quad \text{or} \quad \frac{-3}{4}\,\Omega^4 C^2 (m_j+m_h) \quad \text{when } \omega=\Omega$$

$$\alpha_{14} = -\alpha_{23} = \alpha_{32} = -\alpha_{41} = -m_j m_h \omega^4 K \quad \text{or} \quad -m_j m_h \Omega^4 K \quad \text{when } \omega=\Omega$$

A4.9

and so

$$|R| = \frac{-1}{\nu^8}\,\frac{(m_j+m_h)^2}{m_j^2 m_h^2}\,\omega^6 C^2 \quad \text{or} \quad -\frac{3}{4\nu^8}\,\frac{(m_j+m_h)^2}{m_j^2 m_h^2}\,\Omega^6 C^2 \quad \text{when } \omega=\Omega$$

$$r_{11} = r_{22} = \frac{m_j}{m_h} r_{33} = \frac{m_j}{m_h} r_{44} = \frac{1}{\nu^6}\,\frac{(m_j+m_h)}{m_j m_h^2}\,\omega^4 C^2 \quad \text{or} \quad \frac{3(m_j+m_h)}{4\nu^6 m_j m_h^2}\,\Omega^4 C^2 \quad \text{when } \omega=\Omega$$

$$r_{12} = -r_{21} = \frac{m_h}{m_j} r_{34} = \frac{-m_h}{m_j} r_{43} = \frac{\omega^4 K}{\nu^6 m_j} \quad \text{or} \quad \frac{\Omega^4 K}{\nu^6 m_j} \quad \text{when } \omega=\Omega$$

$$r_{13} = r_{24} = \frac{m_j}{m_h} r_{31} = \frac{m_j}{m_h} r_{42} = \frac{\omega^4 C^2 (m_j+m_h)}{\nu^6 m_h^2 m_j} \quad \text{or} \quad \frac{3(m_j+m_h)\Omega^4 C^2}{\nu^6 m_j m_h^2} \quad \text{when } \omega=\Omega$$

$$r_{14} = -r_{23} = \frac{m_j}{m_h} r_{32} = \frac{-m_j}{m_h} r_{41} = \frac{-\omega^4 K}{\nu^6 m_h} \quad \text{or} \quad \frac{-\Omega^4 K}{\nu^6 m_h} \quad \text{when } \omega=\Omega$$

A4.10

Furthermore

$$r_{11} - \frac{m_j}{m_h} r_{31} = r_{13} - \frac{m_j}{m_h} r_{33} = r_{22} - \frac{m_j}{m_h} r_{42} = r_{24} - \frac{m_j}{m_h} r_{44} = 0$$

$$r_{12} - \frac{m_j}{m_h} r_{32} = -\left\{ r_{21} - \frac{m_j}{m_h} r_{41} \right\}_j = \frac{\omega^4 K (m_j+m_h)}{\nu^6 m_h m_j} \quad \text{or} \quad \frac{\Omega^4 K (m_j+m_h)}{\nu^6 m_h m_j} \quad \text{when } \omega=\Omega$$

$$r_{14} - \frac{m_j}{m_h} r_{34} = -\left\{ r_{23} - \frac{m_j}{m_h} r_{43} \right\}_j = \frac{-\omega^4 K (m_j+m_h)}{\nu^6 m_h^2} \quad \text{or} \quad \frac{-\Omega^4 K (m_j+m_h)}{\nu^6 m_h^2} \quad \text{when } \omega=\Omega$$

A4.11

Hence the linearised response is given by

$$u_1 = \frac{-1}{c(m_j+m_h)} \left\{ \frac{1}{\Omega^2} F_o \sin\Omega t + \frac{K m_j m_h}{c^2(m_j+m_h)} \left[\frac{4m_h}{3m_j\Omega^2} F_o \cos\Omega t - \frac{F}{\omega^2} \cos\omega t \right] \right\}$$

$$u_2 = -\frac{-1}{c(m_j+m_h)} \left\{ -\frac{4}{3c^2\Omega^2} \frac{K m_h^2}{(m_j+m_h)} F_o \sin\Omega t + \frac{1}{\Omega^2} F_o \cos\Omega t + \frac{F}{\omega^2} \cos\omega t \right\}$$

$$u_3 = \frac{-1}{c(m_j+m_h)} \left\{ \frac{1}{\Omega^2} F_o \sin\Omega t + \frac{K m_j m_h}{c^2(m_j+m_h)} \left[\frac{-4}{3\Omega^2} F_o \cos\Omega t + \frac{m_j}{m_h\omega^2} F \cos\omega t \right] \right\}$$

$$u_4 = \frac{-1}{c(m_j+m_h)} \left\{ \frac{4}{3\Omega^2} \frac{K m_j m_h}{c^2(m_j+m_h)} F_o \sin\Omega t + \frac{1}{\Omega^2} F_o \cos\Omega t + \frac{F}{\omega^2} \cos\omega t \right\}$$

A4.12

So that

$$u_1 - u_3 = \frac{-1}{c} \frac{1}{(m_j+m_h)} \frac{K}{c^2} \left\{ \frac{4m_h}{3\Omega^2} F_o \cos\Omega t - \frac{m_j}{\omega^2} F \cos\omega t \right\}$$

$$\dot{u}_1 - \dot{u}_3 = \frac{-1}{c} \frac{1}{(m_j+m_h)} \frac{K}{c^2} \left\{ \frac{-4m_h\Omega}{3\Omega^2\nu} F_o \sin\Omega t + \frac{m_j F\omega}{\omega^2\nu} \sin\omega t \right\}$$

and

$$u_2 - u_4 = \frac{1}{c} \frac{m_h}{(m_j+m_h)} \frac{4K}{3c^2\Omega^2} F_o \sin\Omega t$$

$$\dot{u}_2 - \dot{u}_4 = \frac{4}{3c\Omega^2} \quad \frac{m_h}{(m_j+m_h)} \quad \frac{K\Omega}{c^2\nu} \quad F_o \cos\Omega t$$

A4.13

Thus we find

$$p_1 = Q \left\{ -\left[\frac{4}{3\Omega^2} \right]^2 \frac{1}{4} m_h^2 P_o^2 \Omega \sin 2\Omega t - m_j^2 F^2 \frac{\omega}{2\omega^4} \sin 2\omega t + \frac{4m_j m_h}{3\Omega^2\omega^2} F F_o \frac{1}{2} \left[(\omega+\Omega)\sin(\omega+\Omega)t + (\omega-\Omega)\sin(\omega-\Omega)t \right] \right\}$$

$$p_2 = Qm_h \frac{F_o}{2} \left\{ \left[\frac{4}{3\Omega^2} \right]^2 m_h \Omega F_o (1-2\cos\Omega t) + \frac{4}{3\Omega^2\omega^2} m_j \omega F (\cos(\Omega+\omega)t - \cos(\omega-\Omega)t) \right\}$$

A4.14

where $$Q = \frac{3An_o}{m_j c\nu} \left\{ \frac{K}{cC^2} - \frac{1}{(m_j+m_h)} \right\}^2$$

and the perturbed response is

$$\begin{Bmatrix} V_1 \\ V_2 \\ V_3 \\ V_4 \end{Bmatrix} = -\frac{\nu^2 m_j K}{c^2(m_j+m_h)} \sum_{\substack{\text{resultant} \\ \text{frequencies}}} \frac{1}{\omega^2} \begin{Bmatrix} -m_h P_2 \\ m_h P_1 \\ m_j P_2 \\ -m_j P_1 \end{Bmatrix}$$

A4.15

Finally we find the relative amplitudes of the modulated response compared with those of the fundamental

$$V_i(\omega')_{\text{relative}} = \frac{V_i(\omega') \text{ from A4.15}}{u_i(\omega) \text{ from A4.12}}$$

Considering, for example, the first upper sidebands ($\omega'=\omega+\Omega$) we find

$$\begin{Bmatrix} V_1 \\ V_2 \\ V_3 \\ V_4 \end{Bmatrix}_{\text{relative}} = \frac{3}{2} \frac{F_o n_o K^2 m_h}{c\omega^3 C^3 (m_j+m_h)} \begin{Bmatrix} 1 \\ Km_j m_h / C^2(m_j+m_h) \\ 1 \\ Km_j^2 / C^2(m_j+m_h) \end{Bmatrix}$$

A4.16

DISTRIBUTION

			Copy Number
CS(RN)/DGRA/DNA			1
DES Washington			2
CS(R) 2e			3
CNA/AD/SR	NA223	Dr J.F.Hardenberg	4
	NA226	Dr T.J.Bennett	5
	NA235	Dr A.V.Cooke	6
DG/SM	SM622	Mr R.D.Mulholland	7
ARE(Portland)		N.W.Cooper	8
ARE(Dunfermline)		J.H.Haywood	9
Plessey Marine Research Unit		M.A.Ralph	10
Southampton University - Institute of Sound and Vibration Research		Dr R.Pinnington	11
Y ARD		Dr R.Kinns	12
Vickers Shipbuilding & Engineering Ltd. NAVED		I.Harrison	13
David Brown Gear Industries		Mr Myers	14
ARE(Teddington)		Dr C.J.Jenkins	15
		Mrs L.V.Embling	16
		Mr P Meyer	17
		N1 File	18
DRIC			19-40
ARE(Teddington) File			41-52

END

DATE
FILMED

8-85

DTIC